The ER membrane chaperone Shr3 acts in a progressive manner to assist the folding of related plasma membrane transport proteins

Ioanna Myronidi[§], Andreas Ring[§] and Per O. Ljungdahl*

Department of Molecular Biosciences, The Wenner-Gren Institute, SciLifeLab, Stockholm University, SE-106 91, Sweden

Running title: Membrane-localized chaperone substrate interactions

Keywords: Shr3; membrane-localized chaperone; amino acid permease; polytopic membrane protein folding; endoplasmic reticulum; *Saccharomyces cerevisiae*

[§] Contributed equally, the names are listed in alphabetic order.

[*] Corresponding author. Mailing address: SciLifeLab, Box 1031, SE- 171 21 Solna, Sweden. Phone: 46 8 16 41 01. E-mail: per.ljungdahl@scilifelab.se.

Abstract

Proteins with multiple membrane-spanning segments (MS) co-translationally insert into the endoplasmic reticulum (ER) membrane of eukaryotic cells. In *Saccharomyces cerevisiae*, Shr3 is an ER membrane-localized chaperone that is specifically required for the functional expression of amino acid permeases (AAP), a family of eighteen transporters comprised of 12 MS. Here, comprehensive scanning mutagenesis and deletion analysis of Shr3, combined with a modified split-ubiquitin approach, were used to probe chaperone-substrate interactions with seven different AAP *in vivo*. Our findings indicate that Shr3 specifically recognizes AAP substrates, largely independent of sequence-specific interactions involving membrane and luminally oriented domains. Shr3 selectively and robustly interacts with nested C-terminal AAP truncations in marked contrast to similar truncations of non-Shr3 substrate polytopic sugar transporters. Strikingly, Shr3-AAP interactions initiate with the first 4 MS of AAP and successively strengthen, but abruptly weaken when all 12 MS are present. The data are consistent with Shr3 acting in a temporal manner as a scaffold preventing AAP translation intermediates from engaging in non-productive interactions.

Introduction

The integration and concomitant folding of membrane proteins in the lipid bilayer of the endoplasmic reticulum (ER) are critical steps in the biogenesis of transport proteins destined to function at the plasma membrane (PM). Most eukaryotic membrane proteins are co-translationally inserted into the ER membrane via the Sec61-complex, also known as the translocon. The translocon forms a protein-conducting channel that mediates protein translocation and the co-translational partitioning of membrane-spanning segments (MS) (Johnson and van Waes, 1999; Rapoport et al., 2017; Seinen and Driessen, 2019). During the synthesis of complex polytopic membrane proteins comprised of multiple MS, each MS sequentially exits the channel and partitions into the ER membrane via the lateral gate of the translocon. Although the central channel of the translocon is too small to accommodate multiple MS, the translocon appears to have a limited capacity to promote the folding of membrane proteins comprised of up to three MS; two separate extra-channel MS-binding sites have been reported to act in a chaperone-like manner to delay the release of N-terminal MS until translation is completed (Hou et al., 2012). However, as the complexity of membrane proteins grows beyond three MS, the challenge of preventing inappropriate interactions between incompletely translated nascent chains apparently exceeds the chaperone-like activity of the translocon. Specifically, during the translation of complex polytopic membrane proteins, e.g., amino acid permeases with 12 MS, the N-terminal MS partition into the membrane prior to the synthesis and partitioning of C-terminal MS. To prevent the MS of translation intermediates from entering non-productive folding pathways, discrete and highly specialized ER resident

membrane proteins have been described in fungi that prevent misfolding of specific families of polytopic membrane proteins (Kota and Ljungdahl, 2005; Lau et al., 2000; Ljungdahl et al., 1992; Luo et al., 2002; Martínez and Ljungdahl, 2000; 2004; Sherwood and Carlson, 1999; Shurtleff et al., 2018).

Shr3, the most comprehensively studied of these specialized ER components, was identified as an integral membrane protein required for the functional expression of the conserved family of amino acid permeases (AAP) (Ljungdahl *et al.*, 1992). The AAP family in *Saccharomyces cerevisiae*, belonging to the Amino acid-Polyamine-Organocation (APC) super-family of transporters (Gilstring and Ljungdahl, 2000; Jack et al., 2000; Saier, 2000; Wong et al., 2012), is comprised of 18 genetically distinct but structurally similar proteins with 12 MS. Shr3 is composed of 210 amino acids organized into two functional domains; a N-terminal membrane domain comprised of four hydrophobic α-helices connected by three hydrophilic loops and a hydrophilic cytoplasmically oriented C-terminal domain. Initially, Shr3 was recognized as an essential factor facilitating the packaging of AAP into ER-derived secretory vesicles (Kuehn et al., 1996), and it was found to be important for the proper presentation of ER-exit motifs, located within the hydrophilic C-terminal tails of AAP, to the inner COPII coatomer subunit Sec24 (Kuehn et al., 1998; Malkus et al., 2002; Miller et al., 2002; Miller et al., 2003). Additional data regarding the packaging activity of Shr3 included genetic and physical interactions of Shr3 with components of the COPII-coated vesicles (Gilstring et al., 1999). Also, it was shown that Shr3 facilitated ER-vesicle formation in close proximity to fully integrated and folded AAP (Gilstring and Ljungdahl, 2000; Gilstring *et al.*, 1999) and hence Shr3 was designated a packaging chaperone. The ability of Shr3 to interact with COPII components is primarily linked to its hydrophilic C-terminal tail. Consistently, Shr3 was found to associate with newly synthesized Gap1 in a transient manner, the interaction was reported to exhibit a half-life of approximately 15 min. The observed association with Gap1 was initially thought to occur post-translationally since Gap1 fully integrates into the ER-membrane with each MS correctly oriented independently of Shr3 (Gilstring and Ljungdahl, 2000). Also, the AAP that accumulate in the ER of *shr3*Δ strains do not activate the unfolded protein stress response (UPR) (Gilstring *et al.*, 1999).

However, subsequent studies revealed that Shr3 has an important function that is separate from and precedes its packaging function. Consequently, the view of Shr3 evolved from being a packaging into a specialized membrane-localized chaperone that interacts early with substrate AAP during their co-translational insertion into the ER membrane (Kota et al., 2007; Kota and Ljungdahl, 2005). In these studies, Shr3 was found to prevent the aggregation of AAP in the ER-membrane, a function associated with its N-terminal membrane domain (Kota and Ljungdahl, 2005). Critical evidence demonstrating the importance of Shr3 in facilitating the folding of AAP includes the finding that co-expressed split N- and C-terminal portions of Gap1 assemble into a functional permease in a Shr3-dependent manner (Kota *et al.*, 2007). The

membrane domain of Shr3 is required and suffices to prevent aggregation of the first five MS of Gap1 enabling productive folding interactions with the C-terminal portions of Gap1. Similar to full-length Gap1, the N-terminal fragment displays an increased propensity to aggregate in membranes isolated from cells lacking Shr3, and importantly, its aggregation appeared not to be affected by the presence or absence of the C-terminal fragment. In marked contrast, the aggregation status of the C-terminal fragment was dependent on the presence of both Shr3 and the N-terminal fragment. Since the N- and C-terminal fragments individually insert into the membrane, Shr3 apparently can maintain the N-terminal fragment in a conformation that enables the C-terminal fragment to interact and assemble with it. Although direct physical interactions between Shr3 and substrate AAP have not been demonstrated, all available data is consistent with Shr3 interacting early with N-terminal MS as they co-translationally partition into the ER membrane.

During translocation, exclusively hydrophobic MS partition readily into the lipid phase of the membrane, whereas less hydrophobic MS containing (Heinrich et al., 2000) charged or polar residues partition into the membrane less readily and are retained in proximity to the translocon or to translocon associated proteins, e.g., TRAM (Heinrich and Rapoport, 2003). In analogy to TRAM, we posited that Shr3 facilitates the partitioning of MS of AAP containing charged or polar amino acid residues as they emerge from the translocon. According to this hypothesis, Shr3 may physically shield charged or polar residues within MS, thereby preventing these thermodynamically challenging segments from engaging in nonproductive interactions (Kota *et al.*, 2007). More recent findings in yeast regarding the conserved ER membrane protein complex (EMC) have been interpreted in a similar manner (Miller-Vedam et al., 2020; Shurtleff *et al.*, 2018). However, a striking difference between Shr3 and EMC function is that null alleles of *SHR3* do not activate the UPR (Gilstring *et al.*, 1999).

Despite the clear requirement of Shr3 in AAP biogenesis, we currently lack critical information regarding the mechanisms underlying Shr3 function. Here we have focused on the membrane domain of Shr3 and employed a comprehensive scanning mutagenesis approach to define amino acid residues involved in recognizing AAP substrates. Further, we have exploited a split-ubiquitin approach to directly probe and characterize interactions with seven different AAP substrates *in vivo*. The data support Shr3 acting as a MLC providing a scaffold-like structure to help nascent chains of partially translated AAP maintain a structure required to enter and follow a productive folding pathway as translation proceeds to completion.

Results

Systematic scanning mutagenesis of MS within the membrane domain of Shr3

137 We have previously shown that the membrane domain of Shr3 is required and sufficient for
138 facilitating the folding of AAPs (Kota and Ljungdahl, 2005). Here, a systematic scanning
139 mutagenesis approach was used to identify residues within the Shr3 membrane domain required
140 for function. Intramembrane residues were mutated to leucine; the length of consecutive
141 substitution mutations varied, ranging from 2 to 13 residues. The extramembrane residues
142 within ER lumenal loops L1 and L3 and cytoplasmic oriented NT and loop L2 where mutated
143 to alanine; the length of consecutive alanine replacements ranged from 2 to 3.

144 The biological activity of the mutant proteins was initially assessed using growth-based
145 assays on YPD supplemented with metsulfuron-methyl (MM), which provides a sensitive
146 measure of Shr3 function. MM targets and inhibits branched-chain amino acid synthesis and
147 growth is strictly dependent on the combined activity of multiple SPS-sensor regulated AAP
148 that facilitate high-affinity isoleucine, leucine and valine uptake (Andréasson and Ljungdahl,
149 2002; Jørgensen et al., 1998). Serial dilutions of cell suspensions from strain JKY2 (*shr3*Δ)
150 carrying vector control (VC), *SHR3* or the *shr3* mutant alleles were spotted on YPD and
151 YPD+MM plates (Supplementary Material Fig. S1 – S10). Only three mutant alleles, *shr3-35*,
152 *shr3-50* and *shr3-76*, failed to support growth (Fig. 1A and B). The steady state levels of the
153 three mutant proteins were similar to wildtype Shr3 (Fig. 1B), suggesting that the mutant
154 proteins were not grossly misfolded, and consequently, not prematurely targeted for ER-
155 associated degradation.

156 The *shr3-35* allele encodes a protein with residues 17 through 19 (serine-alanine-threonine)
157 in MS I replaced by leucine (Fig. 1A). To more precisely define the critical residues, we
158 constructed additional mutant alleles with paired leucine substitutions at residues 17-18 (LLT),
159 18-19 (SLL), and 17 and 19 (LAL). Expression of *SHR3-36* (LLT) and *SHR3-38* (LAL) alleles
160 complemented *shr3*Δ and supported wildtype growth on YPD + MM (Fig. 1C, dilutions 4 and
161 6). By contrast, cells expressing *shr3-37* (SLL) did not complement, exhibiting a phenotype
162 similar to the *shr3-35* (LLL) mutant (Fig. 1C, dilutions 3 and 5).

163 The *shr3-76* allele carries leucine replacements at residues 139 through 142 (serine-
164 asparagine-isoleucine-isoleucine) in MS IV (Fig. 1A). Again, the importance of the affected
165 residues was tested by creating alleles with paired leucine substitutions at positions 139-140
166 (LLII) and 141-142 (SNLL). Cells expressing *shr3-77* (LLII) allele grew poorly, although
167 slightly better than cells expressing the *shr3-76* allele (Fig. 1C, dilutions 15 and 16). Cells
168 expressing *SHR3-78* (SNLL) grew as wildtype *SHR3* (Fig. 1C, dilutions 14 and 17).

169 The third non-functional allele, *shr3-50*, encodes a mutant protein with alanine
170 substitutions at residues 51 through 53 (leucine-arginine-histidine) located within the ER
171 lumenal loop L1 (Fig. 1A). The importance of these residues was tested by paired alanine
172 substitutions of the positions 51-52 (AAH), 52-53 (LAA), and 51 and 53 (ARA). Expression of
173 these alleles demonstrated that *SHR3-51* (AAH) and *SHR3-52* (LAA) complemented *shr3*Δ

similar to wildtype *SHR3* (Fig.1C, dilutions 8, 10 and 11). The *shr3-53* (ARA) allele exhibited reduced growth (Fig. 1C, dilution 12), indicative of compromised function. The finding that mutations affecting residues 53-55 in the ER lumenal loop L1 abolish function suggests that extramembrane sequences are important for guiding the folding of AAP sequences destined to be oriented towards the extracellular side of the PM.

Deletion analysis of ER-lumen oriented loops

The possibility that Shr3 engages and interacts with its substrate AAP through contacts with extramembrane sequences prompted us to specifically test the functional significance of loops L1 and L3 (Fig. 2A). The residues 44-57 within L1 are predicted to fold into an amphipathic α-helix (Fig. 2B). We constructed four internal deletions in L1 that affect this secondary structure motif to varying extent: *shr3Δ90* (Δ34-48); *shr3Δ91* (Δ39-47); *shr3Δ92* (Δ44-54); and *shr3Δ93* (Δ55-60). Also, an internal deletion in L3 was constructed: *SHR3Δ94* (Δ121-127). The five deletion alleles directed the expression of mutant proteins at levels comparable to *SHR3* (Fig. 2C); the deletions do not decrease the steady state levels of protein. The function of these deletion alleles was assessed as before using YPD + MM. We also extended the analysis with more nuanced growth-based assays capable of monitoring amino acid uptake catalyzed predominantly by a single or a couple of AAP. This was accomplished by examining growth on minimal media individually supplemented with toxic amino acid analogues D-histidine, L-canavanine, and azetidine-2-carboxylate (AzC), which are taken up by Gap1 (Gresham et al., 2010), Can1 (Ono et al., 1983), Agp1/Gnp1 (Andréasson et al., 2004), respectively. The expression of functional alleles of *SHR3* results in impaired growth in the presence of these toxic analogues. Serial dilutions of cell suspensions from strain JKY2 (*shr3*Δ) carrying vector control (VC), *SHR3*, *shr3Δ90*, *shr3Δ91*, *shr3Δ92*, *shr3Δ93* or *SHR3Δ94* were spotted on SAD containing D-histidine, SD + L-canavanine, SD + AzC, and YPD + MM plates. The four internal deletion alleles affecting L1 failed to complement *shr3*Δ; the strains grew similar as the VC (Fig. 2C, dilutions 1, 3, 4, 5 and 6). By contrast, the strain expressing the internal deletion in L3 showed a more complex pattern of growth. On SAD + D-histidine and SD + L-canavanine, *SHR3Δ94* appeared to express a non-functional protein, the strain grew in the presence of these toxic amino acid analogues (Fig. 2C, compare dilution 1 with 7). However, on SD + AzC and YPD + MM, the *SHR3Δ94* allele exhibited growth similar to wildtype *SHR3* (Fig. 2C, compare dilution 2 with 7). Note that on YPD + MM the strain carrying *SHR3Δ94* exhibited enhanced growth compared to wildtype, and consequently, on YPD + MM we designated the phenotype WT^{+}.

Lumenal loop L3 influences substrate specificity

210 The finding that *SHR3Δ94* exhibited a range of phenotypes, i.e., from null to apparently
211 enhanced functionality, prompted us to reexamine the growth characteristics of the 44 leucine-
212 and alanine-scanning mutant alleles using the more nuanced growth-based assays. Serial
213 dilutions of cell suspensions from strain JKY2 (*shr3*Δ) carrying vector control (VC), *SHR3* or
214 one of the individual mutant alleles were spotted on SAD + D-histidine, SD + L-canavanine,
215 SD + AzC and YPD+MM (Supplementary Material Fig. S1-S10). The growth characteristics
216 were evaluated and the results, including the internal loop deletions, are summarized in an
217 ordered heat-map (Fig. 3A). As was found in the initial evaluation of growth on YPD+MM,
218 most of the mutant alleles were judged to encode functional proteins; the strains grew similarly
219 as the strain carrying the *SHR3* wildtype control. Reevaluation of the three non-functional
220 alleles, *shr3-35*, *shr3-50* and *shr3-76*, confirmed that the mutations exhibit major defects on all
221 of the selective media (Fig. 3A). However, in some instances, several of the mutations, similar
222 to *SHR3Δ94*, conferred robust growth on YPD+MM but did not complement *shr3*Δ on the other
223 selective media. Strikingly, *SHR3-45*, *-63*, *-65*, *-68*, *-71*, *-74*, and *-75*, supported more robust
224 growth on YPD + MM than *SHR3*, but exhibited a null phenotype on media containing toxic
225 amino acid analogues. In summary, growth in the presence of D-histidine was found to be the
226 most sensitive monitor of mutations in *SHR3*, perhaps due to the fact that D-amino acids are
227 taken up by a single AAP, Gap1 (Grenson et al., 1970; Rytka, 1975). We note that mutations
228 localized to the MS III and IV and the ER lumenal oriented loop L3 exhibited the most
229 pleiotropic affects, suggesting that these regions of Shr3 facilitate interactions with discrete
230 AAP, and potentially, comprise substrate specific determinants.

231 We performed multiple sequence alignments of the membrane domain of Shr3 and orthologs
232 from two *Saccharomyces sensu stricto* strains, *S. paradoxus* and *S. mikatae*, and from three
233 divergent *lato* fungal strains, *Candida albicans* (Csh3), *Schizosaccharomyces pombe* (Psh3)
234 and *Aspergillus nidulans* (ShrA) and obtained a consensus identity plot (Fig. 3B) (Madeira et
235 al., 2019). The Shr3 orthologs of *C. albicans, S. pombe* and *A. nidulans* have been shown to
236 function analogously and are required for proper amino acid uptake. Heterologous expression
237 of *CSH3* complements *shr3*Δ (Martínez and Ljungdahl, 2004), whereas heterologous
238 expression of *PSH3* or *SHRA* only partially complement *shr3*Δ, merely facilitating the
239 functional expression of limited subset of permeases (Erpapazoglou et al., 2006; Martínez and
240 Ljungdahl, 2000). The Shr3 sequence is well-conserved in the *Saccharomyces sensu stricto*
241 strains, exhibiting almost absolute identity. Several positions throughout the membrane domain
242 of Shr3 are conserved between the full set of selected sequences. Interestingly, threonine 19,
243 which is the single critical amino acid residue in MS I, is conserved in all orthologs (Fig. 3B,
244 T19 is highlighted in dark blue). The requirement for a polar amino acid in MS IV of Shr3 is
245 conserved as well (Fig. 3B, S139 highlighted in dark blue). A higher sequence divergence is
246 evident in the luminal loop L3, with the extreme case of the *A. nidulans* orthologue that contains
247 an extra sequence of twelve amino acid residues. The limited sequence identity in loop L3

248 aligns with the observation that mutations in L3 of Shr3 exhibit the most pleiotropic effects,
249 and is consistent with the notion that L3 affects substrate specificity.

250 The finding that the Shr3Δ94 mutation supported robust growth on YPD+MM, suggested
251 that the mutant protein retained the capacity to facilitate Ssy1 folding. In contrast to the other
252 members of the AAP transporter family, Ssy1 functions as the primary receptor of extracellular
253 amino acids in the context of the plasma membrane-localized SPS sensor (Didion et al., 1998;
254 Iraqui et al., 1999; Klasson et al., 1999). In response to extracellular amino acids, Ssy1 initiates
255 signaling events leading to the proteolytic activation of Stp1, which in turn induces the
256 expression of several AAP genes including *AGP1* and *GNP1* and multiple permeases
257 facilitating branched amino acid uptake. As an indirect measure of Shr3-Ssy1 interactions, we
258 examined the proteolytic cleavage of the transcription factor Stp1 (Fig. 3C). Consistent with
259 the growth assays, leucine induction led to Stp1 processing in strain FGY135 (*shr3*Δ)
260 expressing *SHR3* or *SHR3Δ94* (Fig. 3C, lanes 4 and 8), but not the non-functional alleles *shr3-*
261 *35*, *shr3-50* or *shr3-76* (Fig. 3C, lanes 6, 10 and 12).

262

263 **Shr3-AAP substrate interactions**

264 To test if the observed growth phenotypes of the mutated *SHR3*/*shr3* alleles correlated with the
265 ability of mutant Shr3/shr3 proteins to interact with specific AAP and facilitate their functional
266 expression we exploited a split-ubiquitin approach to monitor Shr3-AAP interactions *in vivo*
267 (Fig. 4A and 4B). A sequence encoding the N-terminal fragment of ubiquitin carrying the I13A
268 mutation (NubA), which reduces the propensity of non-specific interactions (Johnsson, 2002;
269 Johnsson and Varshavsky, 1994), was fused at the C-terminal end of *SHR3*, *shr3-35*, and
270 *SHR3Δ94*, creating the Shr3-NubA constructs schematically depicted in Fig. 4A. Next, we
271 created a *GAP1* allele encoding the C-terminal fragment of ubiquitin (Cub) tagged with GST-
272 6xHA (Cub-GST) (Fig. 4A). The resulting *GAP1-Cub-GST* was placed under the control of the
273 *GAL1*-promoter. When co-expressed, productive interactions between Gap1 and Shr3 enable
274 the split NubA and Cub domains to assemble a functional ubiquitin moiety that is recognized
275 by ubiquitin-specific proteases, resulting in the release of the GST-6xHA reporter (Fig. 4B).
276 The functional attributes of the NubA fusion constructs were tested by their ability to
277 complement *shr3*Δ (Fig. 4C, dilutions 3-5); strains carrying *SHR3-NubA* or *SHR3Δ94-NubA*
278 grew as well as *SHR3* without NubA (Fig. 4C, compare dilution 2 with 3 and 5), whereas the
279 *shr3-35-NubA* allele did not (dilution 4). The *GAP1-Cub-GST* allele encodes a functional Gap1
280 protein that facilitates citrulline uptake as well as wildtype Gap1 (Fig. 4C, compare dilution 7
281 with 8). The functionality of Gap1-Cub-GST is dependent on its ability to exit the ER; a
282 construct lacking the ER exit motif in the hydrophilic C-terminal domain of Gap1 is not
283 functional (Fig. 4C dilution 9), presumably due its retention in the ER.

To test *in vivo* interactions, we analyzed protein extracts from strain FGY135 (*shr3*Δ *gap1*Δ) carrying plasmids *GAP1-Cub-GST* and *SHR3-NubA*, *shr3-35-NubA* or *SHR3*Δ*94-NubA* using anti-HA immunoblot analysis. In cells expressing *SHR3-NubA* or *SHR3*Δ*94-NubA* and *GAP1-Cub-GST-6xHA*, two bands were detected, corresponding to full-length Gap1-Cub-GST-6xHA and the cleaved GST-6xHA (Fig. 4D, lane 1). We calculated the fraction of split-ubiquitin cleavage in the *SHR3-NubA* strain to be ≈ 20% by dividing the intensities of the cleaved band with the intensities from full-length plus cleaved species; whereas in the *SHR3*Δ*94-NubA* strain the cleavage was 5% (Fig. 4D); By contrast, only a single band, full-length Gap1-Cub-GST-6xHA, was detected in extracts from the strain expressing the non-functional *shr3-35-NubA* and *GAP1-Cub-GST-6xHA* constructs (Fig. 4D, lane 2). Although expressed at similar levels, the ER retained gap1-ERX$_{AAA}$-Cub-GST protein did not exhibit an enhanced propensity to interact with Shr3, suggesting the split-ubiquitin assay primarily monitors transient interactions during AAP biogenesis (Fig. S11).

Based on the success of the split ubiquitin approach to analyze Shr3-Gap1 interactions, we created Cub-GST-6xHA tagged constructs with five additional AAP, i.e., Agp1, Gnp1, Bap2, Can1 and Lyp1, the non-transporting but Shr3-dependent AAP homologue Ssy1 (Klasson *et al.*, 1999), and two Shr3-independent sugar transporters (HXT), i.e., the low-affinity glucose transporter Hxt1 and the galactose transporter Gal2 (Fig. 5A). Extracts from strain FGY135 (*shr3*Δ *gap1*Δ) carrying *SHR3-NubA*, *shr3-35-NubA* or *SHR3*Δ*94-NubA* and a single *AAP-Cub-GST-6xHA* or *HXT-Cub-GST-6xHA* construct were prepared and the levels of the GST-6xHA reporter were determined (Fig. 5B-E). Consistent with the general requirement of Shr3 for AAP folding, robust interactions were detected between Agp1-, Gnp1-, Bap2- and Ssy1-Cub constructs and wildtype Shr3-NubA (Fig. 5B, C). Although Shr3 is required for their functional expression, Can1- and Lyp1-Cub constructs exhibited low levels of reporter cleavage, similar to the Shr3-independent sugar transporters (Fig. 5D, E). These latter observations are consistent with Shr3 functioning in a transient manner, primarily interacting with AAP substrates during early stages of AAP folding. In the context of full-length AAP, the split-ubiquitin signal may reflect weaker post-folding interactions.

AAP-Cub interactions with shr3-35-NubA were weak or absent, which is precisely aligned with it being non-functional on all selective media tested (Fig. 1, 3). Unexpectedly, the split-Ub interactions with unrelated sugar transporters (HXT) were also weaker compared to the wildtype Shr3-NubA (Fig. 5E). This prompted us to test the trivial explanation that the NubA domain of Shr3-35-NubA is incorrectly oriented. The NubA is correctly oriented to the cytoplasm and thus in a context capable of supporting potential interactions (Supplementary Material, Fig. 12A). Together these findings indicate that the shr3-35 protein, although expressed at similar levels as Shr3, is incapable of engaging in both specific and non-specific secretory substrate interactions.

321 Interestingly, the Shr3Δ94-NubA interacted with all AAP-Cub constructs, but at
322 significantly reduced levels, and consequently, the data did not explain the enhanced growth
323 conferred by the *SHR3Δ94* allele on YPD + MM (Fig. 2 and 3). In marked contrast, Shr3Δ94-
324 NubA interacted with Ssy1-Cub-GST-6xHA at levels comparable to Shr3-NubA (Fig.5 C),
325 which provided the mechanistic explanation for the enhanced growth phenotype. Ssy1 is a
326 unique member of the AAP family that strictly requires Shr3 for folding (Klasson *et al.*, 1999)
327 and constitutes the integral membrane component of the PM-localized SPS sensor that induces
328 the expression of AAP genes in response to extracellular amino acids (Ljungdahl and Daignan-
329 Fornier, 2012). Apparently, the Shr3Δ94 mutant retains ability to assist the folding of Ssy1,
330 restoring the transcriptional circuits abrogated by *shr3*Δ. Consistent with this notion, the
331 Shr3Δ94 allele supports Stp1 processing (Fig. 3C). The induced expression of multiple AAP
332 that facilitate branched-chain amino acid uptake correlates well with the growth-based
333 phenotypes. Together, the results indicate that the *in vivo* interactions monitored by the split
334 ubiquitin cleavage provide a nuanced assessment of Shr3 function.

335

336 **Shr3 interacts with substrates in a progressive manner**

337 As a proxy to investigate the temporal aspects of Shr3-facilitated AAP folding, we constructed
338 a series of truncated *gap1-Cub-GST, hxt1-Cub-GST* and *gal2-Cub-GST* alleles capable of
339 encoding 2, 4, 6, 8, 10 and 12 MS (Fig. 6A). Strain FGY135 (*shr3*Δ *gap1*Δ) carrying plasmid
340 *SHR3-NubA* and a truncated *gap1-Cub-GST, hxt1-Cub-GST* or *gal2-Cub-GST* allele was
341 employed and potential interactions were monitored by immunoblot. Shr3-NubA did not
342 interact with gap1-2TM, even though the Cub domain is presented in the context of proper
343 membrane topology oriented towards the cytoplasm (Supplementary Material, Fig. S12 B). The
344 presence of two additional MS of Gap1 (gap1-4TM) supported an interaction with Shr3 (Fig. 6
345 B left panel, C in black). The intensity of the interactions increased and eventually plateaued in
346 the strains carrying the *gap1-6TM/-8TM/-10TM* alleles, respectively (Fig. 6 B left panel, C in
347 black). Strikingly, the gap1-12TM construct interacted only weakly with the functional Shr3-
348 NubA (Fig. 6 B left panel, C in black). In marked contrast to the interaction pattern of the gap1-
349 Cub-GST truncations with Shr3-NubA, we could not detect the GST-6xHA reporter in extracts
350 from the strain expressing *SHR3-NubA* and any of the truncated *hxt1-Cub-GST* or *gal2-Cub-*
351 *GST* alleles (Fig. 6B, center and left panel, C in grey and white). These findings support the
352 notion that our split ubiquitin approach is suitable to monitor specific Shr3-AAP interactions.
353 As a critical test, we examined if robust interactions could be detected between Shr3-NubA and
354 two truncated Can1 constructs with eight and ten MS (Fig. S13). The rational being that growth-
355 based and biochemical assays have clearly defined Can1 as a *bona fide* substrate of Shr3.
356 However, interactions between full-length Can1 and Shr3 are weak, similar to that
357 corresponding to the non-Shr3 substrates Hxt1 and Gal2 (Fig. 5D and E). We posited that if

358 truncations of AAP are indeed proxies of translation intermediates, then truncations of Can1
359 would readily interact with Shr3. Interactions between the can1-8TM and -10TM Cub
360 constructs with Shr3-NubA were readily detected (Fig. S13 B, C), findings clearly consistent
361 with Shr3 functioning at early stages of AAP biogenesis.

362 To more fully understand Shr3-substrate interactions, we created a series of truncated Agp1
363 and Ssy1 split-ubiquitin constructs (Fig. 7A). Interestingly, in contrast to gap1-2TM, the agp1-
364 2TM construct clearly interacted with Shr3-NubA (Fig. 7A; black bars). Aside from this
365 difference, the pattern of interactions with the remaining Agp1 constructs was strikingly similar
366 to that observed with Gap1 truncations; the intensity of the GST-6xHA reporter increased
367 successively as the number of MS increased from 4 to 10, and greatly reduced when all 12 TM
368 were present (Fig. 7A, black bars). The interactions of the Shr3Δ94-NubA with the agp1-Cub
369 constructs followed a similar pattern to that of the wildtype Shr3-NubA, albeit of lower intensity
370 (Fig. 7A, white bars). Notedly, the interaction pattern with the Ssy1 constructs was quite
371 different (Fig. 7B). Interestingly, as did agp1-2TM, the ssy1-2TM interacted with Shr3-NubA,
372 strongly suggesting that Shr3 engages early during the biogenesis of Ssy1. The ssy1-4TM and
373 -6TM constructs exhibited weaker interactions, however, the ssy1-8TM, -10TM and -12TM
374 constructs exhibited robust interactions. As anticipated from growth-based assays, Shr3Δ94-
375 NubA exhibited an interaction pattern very similar to the wildtype Shr3-NubA construct.

376

377 ## Discussion

378 The biogenesis of AAP can be divided into three interconnected but discrete functional steps:
379 1) co-translational partitioning and integration into the ER membrane; 2) folding into native
380 structures; and 3) packaging into ER-derived COPII-coated transport vesicles. Shr3 is not
381 essential for integration (Gilstring and Ljungdahl, 2000), but is required for folding and
382 packaging into COPII-coated vesicles (Gilstring *et al.*, 1999; Kuehn *et al.*, 1998; Kuehn *et al.*,
383 1996); Kota and Ljungdahl, 2005;(Kota *et al.*, 2007; Kota and Ljungdahl, 2005). Here, our
384 studies were aimed at further elucidating the role of Shr3 in facilitating AAP folding, i.e. its
385 membrane-localized chaperone (MLC) function.

386 Saturation scanning mutagenesis of the N-terminal membrane domain of Shr3 allowed us
387 to define amino acid residues that are critical for the recognition of AAP as folding substrates
388 (Supplementary Material Fig. S1-S10; Fig. 3A). Strikingly, mutations affecting a few amino
389 acids residues at three discrete sites resulted in a complete loss of function, suggesting that Shr3
390 generally recognizes its folding substrates independently of sequence-specific interactions, but
391 rather based on the presence of structural determinants shared by the AAP. The critical residues
392 identified in MSI and MSIV shared the common feature of being polar (Fig. 1C). Threonine19
393 is conserved among closely and more distant fungal species (Fig. 3B), and it is of interest to
394 note that one of the original spontaneous mutations that led to the identification of *SHR3* is a

395 T19R mutation (Ljungdahl *et al.*, 1992). Strikingly, two mutant proteins carrying 10
396 consecutive leucine residues (aa 62-71, Shr3-57, MSII) or 9 (aa 145-153, Shr3-79, MSIV)
397 support functional expression of AAP in manner indistinguishable from wildtype Shr3, and the
398 Shr3-58 mutant with 13 consecutive leucine residues (aa 69-81, MSII) functions well for all
399 AAP except Gap1 (Fig. 3A, Fig. S6). These findings suggest that hydrophobic interactions
400 between MS of Shr3 and AAP can develop even at the expense of larger sections of specific
401 Shr3 sequence, presumably provided that its overall membrane structure is retained. The data
402 are consistent with Shr3 acting as a scaffold for AAP folding, a function that primarily depends
403 on hydrophobic interactions but with the capacity to shield energetically unfavorable polar
404 residues of AAP MS. Importantly, exposed polar residues may be recognized by a hydrophilic
405 pocket identified in the structure of the ERAD-associated E3 ubiquitin ligase Hrd1 (Schoebel
406 et al., 2017), which participates in the degradation of misfolded AAP in cells lacking Shr3 (Kota
407 *et al.*, 2007).

408 The finding that one of the three loss-of-function mutations disrupting Shr3 function
409 resides in the lumen-oriented loop L1 (Fig. 1) suggests that the role of Shr3 as a MLC is not
410 restricted to MS-mediated hydrophobic interactions. Apparently, Shr3 facilitates the folding of
411 AAP in a manner dependent on extramembrane lumen-oriented sequences. Consistent with this,
412 all internal deletions in L1 of Shr3 strongly affected its function (Fig. 2). Interestingly, L1
413 contains a predicted α-helical structure with amphipathic characteristics (aa 44-57) that is
414 disrupted in each of the internal deletion mutant proteins.

415 By contrast to mutations affecting L1, the deletion affecting L3 (*SHR3Δ94*) exhibited a
416 variable effect on amino acid uptake (Fig. 2), a phenotype that we could trace to differential
417 interactions with distinct AAP substrates. Consequently, the data implicate L3 as an important
418 determinant that influences substrate interactions. This region appears to be critical for
419 interactions with Gap1 and Can1, but less important for interactions with Agp1/Gnp1, and
420 clearly dispensable for interactions with Ssy1 (Fig. 2, Fig. 4, Fig. 5). Consistently, some
421 mutations in *SHR3* result in WT+ phenotypes, i.e., exhibiting more robust growth than wildtype
422 (Fig. 3A). This latter gain-of-function phenotype is presumably due to proper Ssy1 folding;
423 cells that carry these mutations remain capable of inducing AAP gene expression in a manner
424 that is augmented by the derepression of nitrogen regulation (Ljungdahl and Daignan-Fornier,
425 2012). Thus, under the specific growth conditions used, cells carrying L3 mutations express
426 enhanced levels of AAP leading to WT+ growth phenotype.

427 The observation that Ssy1, the only non-transporting AAP, exhibits a lax requirement for
428 L3 to fold, suggests that transporting AAP may have an enhanced requirement for the chaperone
429 function of Shr3. This notion is consistent with recent evidence showing that extracellular loops
430 of AAP are not merely MS-connecting sequences but rather have important roles affecting
431 intracellular trafficking and transport function (van't Klooster et al., 2020). Some of the

432 hydrophilic loops of AAP are of considerable length, especially extracellular loops 3 and 4
433 connecting MS V-VI and VII-VIII, respectively. Secondary structure predictions suggest the
434 extracellular loop 4 of the lysine permease Lyp1 (van't Klooster *et al.*, 2020) and Gap1
435 (Ghaddar et al., 2014a) possesses α-helical regions that appear to influence the substrate
436 specificity of amino acid transport (Risinger et al., 2006). Consistent with a requirement for the
437 lumen-oriented loops of Shr3, the loop regions of AAP that face the extracellular milieu are
438 lumen-oriented during biogenesis. Interactions between the lumen-oriented loops of Shr3 may
439 prevent precocious folding of the extracellular loops, maintaining them in a more flexible state
440 required for subsequent folding events, e.g., involving MS that fold in a context with more
441 distal C-terminal MS. In analogy, proper trafficking and functional expression of the closest
442 AAP homologues in mammals, the L-type amino acid transporters (LAT) (SLC7 family)
443 depend on extramembrane region-mediated recognition by the 4F2hc, or rBAT, members of
444 the SLC3 protein family (Fotiadis et al., 2013). The extracellular orientation of the interacting
445 regions upon plasma-membrane localization of the SLC7-SLC3 holo-LAT transporters in in
446 line with the concept of extramembrane regions containing motifs for substrate recognition and
447 specificity exhibited by amino acid transporter biogenesis factors (Rosell et al., 2014).

448 Although there is no crystal structure of an AAP, Bap2 (Usami et al., 2014), Can1 (Ghaddar
449 *et al.*, 2014a), Gap1 (Ghaddar et al., 2014b) and Tat2 (Kanda and Abe, 2013) have been
450 successfully modeled onto the *E. coli* arginine/agmatine antiporter AdiC (Gao et al., 2010).
451 AdiC has 12 MS and belongs to the Amino Acid-Polyamine-Organocation (APC) super-family
452 of transporters. The 12 MS are arranged in a 5+5 inverted repeat fold that form the transporter
453 core, with MS XI and XII appearing to hold the two halves together. MS I, III, VI, VIII and X
454 shape the binding pocket. To directly probe the *in vivo* interactions between Shr3 and AAP we
455 adapted and applied a split-ubiquitin approach that is independent of a transcriptional readout.

456 In the context of full-length AAP, we found that the split-ubiquitin signal was relatively
457 weak, specifically in comparison to the signals with truncated substrates. Also, we detected
458 low levels of interactions with full length non-Shr3 substrates that do not rely on Shr3
459 chaperone function for folding, indicating that the split-ubiquitin approach is sensitive and
460 accurately reflects biologically relevant interactions. Perhaps, Shr3 can interact with many
461 secretory substrates but some interactions become stronger and specific when structural
462 characteristics distinct from the general ones are involved. In support of this notion, the pattern
463 of interactions between Shr3 and truncated Gap1, Agp1, Can1 and Ssy1 is striking, particularly
464 in contrast to truncated HXT (Hxt1 and Gal2) exhibiting essentially no interactions (Fig. 6, 7,
465 and S13). The specific interactions with AAP were detected when only the first 2 to 4 MS were
466 present. As more MS were added the interactions increased and plateaued until MS XI and XII
467 were present, at which point the interactions significantly lessen. By contrast, full-length (Fig.
468 5) and 12MS truncated (Fig. 7) forms of Ssy1 exhibited more persistent interactions with Shr3
469 and Shr3Δ94, perhaps attributable to Ssy1 being substantially larger than transporting AAP.

470 Together, the data we acquired in this study provide further support to our previously
471 described model (Kota *et al.*, 2007; Kota and Ljungdahl, 2005) whereby Shr3 transiently
472 interacts with AAP early as their MS partition into the ER membrane, acting as an assembly
473 site for MS helices. This activity is required to prevent AAP translation intermediates from
474 engaging in nonproductive interactions, shielding polar residues, until all MS are available and
475 presented in a context of the long-range intramolecular interactions inherent to the native 3D-
476 structure of AAP (Fig.8). Our model for the Shr3 chaperone function in the biogenesis of AAP
477 is analogous to that of the bacterial insertase/chaperone YidC (Beck et al., 2001; (Dalbey and
478 Kuhn, 2014) acting as an assembly site for alpha helices in the folding of LacY whereby
479 hydrophobic interactions mediate shielding of LacY to provide a protective chamber that
480 reduces energetically unfavorable contacts in the non-native structure during translation
481 (Nagamori et al., 2004; Serdiuk et al., 2016; Serdiuk et al., 2019; Wagner et al., 2008; Zhu et
482 al., 2013). Similar transient MLC-substrate interactions have been reported in the case of the
483 mammalian PAT intramembrane chaperone complex, comprised of four MS, three contributed
484 by Asterix and one by CCDC47 (Chitwood and Hegde, 2020). Although in these studies an *in*
485 *vitro* translation system was employed, in contrast to our *in vivo* split-ubiquitin approach, the
486 PAT complex interaction was found to be selective for truncated, immature β1-adrenergic
487 receptor constructs compared to the full-length substrate, which presumably is capable of helix
488 packing and polar residue shielding.

489 The chaperone-like capacity of the conserved eukaryotic ER membrane protein complex
490 (EMC) insertase has recently been explored (Bai et al., 2020; O'Donnell et al., 2020; Pleiner et
491 al., 2020; Volkmar and Christianson, 2020). The results point to EMC acting in close proximity
492 with nascent polytopic membrane proteins typically enriched for MS containing polar or
493 charged residues, shielding them from degradation during folding (Miller-Vedam *et al.*, 2020;
494 Shurtleff *et al.*, 2018). Importantly, the EMC can associate with a number of ER-integral
495 substrate-specific chaperones such as Sop4 (Luo *et al.*, 2002), Gsf2 (Kota and Ljungdahl, 2005;
496 Sherwood and Carlson, 1999) and Ilm1 (Shurtleff *et al.*, 2018). Shr3, although an abundant ER
497 membrane protein, has not been identified as an interacting partner of EMC components
498 (Shurtleff *et al.*, 2018). Potentially, Shr3 and the EMC act in proximity to distinct ribosome
499 populations, functioning in a parallel manner, enabling the Sec61 translocon to pair with diverse
500 and distinct sets of partners, and thereby facilitate the efficient biogenesis of more challenging
501 versus canonical substrates of the secretory pathway (O'Keefe and High, 2020).

502 In the case of Shr3, the early interactions with nascent AAP being inserted in the lipid
503 bilayer together with the ability of Shr3 to interact with COPII components via its C-terminal
504 cytoplasmic tail (Gilstring *et al.*, 1999), converge to function as a nexus between AAP folding
505 and packaging into COPII-coated vesicles. The potential network of dynamic interactions in
506 the ER remains to be explored for an integral substrate-specific chaperone as well as what
507 structural determinants in the substrates dictate a remarkable degree of substrate specificity. To

508 this end, the broad collection of mutations that we have acquired in combination to our extended
509 growth-based phenotype analysis and in vivo interaction studies lay the ground for future
510 structural studies that are required to gain insights into the mechanistic details that underlie this
511 substrate-specific MLC function.

512

513 Materials and methods

514 Yeast strains and plasmids

515 Yeast strains and plasmid used are listed in Supplementary Material Tables S1 and S2,
516 respectively.

517

518 Media

519 Standard media, YPD (yeast extract, peptone, dextrose), SD (synthetic defined with ammonium
520 as nitrogen source and glucose as carbon source) were prepared as previously described (Burke
521 et al., 2000). Ammonia-based synthetic complete dextrose (SC) drop-out medium, were
522 prepared as described (Andréasson and Ljungdahl, 2002) and SAD (synthetic minimal
523 dextrose, with allantoin as sole nitrogen source) was prepared as previously described. Media
524 were made solid with 2% (wt/vol) bacto Agar (Difco), 2% (wt/vol) washed bacto Agar (Difco)
525 or 2% (wt/vol) washed pure Agar where indicated. Sensitivity to 200 µg/ml MM (2-{[({[(4-
526 methoxy-6-methyl)-1,3,5-triazin-2-yl]-amino}carbonyl) amino-]-sulfonyl}-benzoic acid) was
527 tested on YPD as described previously (Jørgensen *et al.*, 1998). Sensitivity to 1 mM AzC
528 (azetidine-2-carboxylate), 10 µg/ml DL-ethionine, 50 µg/ml p-Fluoro-DL-phenylalanine and 1
529 µg/ml L-canavanine was tested on SD. Sensitivity to 0,5% (wt/vol) D-histidine was tested on
530 SAD media made solid with washed pure Agar. Cells were grown over night in SC-uracil
531 medium, cells were then resuspended in water to OD=1, 10-fold dilutions were prepared in
532 water and then spotted on the indicated medium. Plates were then incubated at 30°C for 2–3 d
533 and photographed. Gap1-dependent citrulline uptake was monitored on minimal medium
534 containing 2 % galactose as carbon source, 1 mM L-citrulline as sole nitrogen source and uracil.
535 Media were made solid with washed bacto Agar. Plates were incubated at 30 °C for 7 d and
536 photographed.

537

538 Immunoblot analysis

539 Whole-cell extracts were prepared under denaturing conditions using NaOH and trichloroacetic
540 acid as described previously (Silve et al., 1991). Proteins were separated using SDS-PAGE and
541 blotted onto Amersham Protran 0.45 µm nitrocellulose membrane (GE Healthcare). The
542 primary antibodies and dilutions were, mouse anti-Dpm1 5C5A7 (Abcam), 1:2500; rat anti-

543 HA-HRP 3F10 (Roche Applied Science), 1:2500-1:5000; mouse anti-Pgk1 22C5D8 (Thermo
544 Fisher Scientific), 1:10000 and rabbit anti-Shr3, 1:9000. Secondary antibodies and dilutions
545 used were, goat anti-mouse-poly-HRP (Thermo Fisher Scientific), 1:5000 and goat anti-rabbit-
546 poly-HRP (Thermo Fisher Scientific), 1:5000. Immunoreactive bands were visualized by
547 chemiluminescence using (SuperSignal West Dura Extended-Duration Substrate; Thermo
548 Fisher Scientific) as substrate in a ChemiDoc imaging system (Biorad).

549

550 **Split-ubiquitin assay**

551 Cells were pre-grown in SD+R (synthetic defined with ammonium as nitrogen source and 2 %
552 raffinose and 0.1 % glucose as carbon source) to logarithmic phase. Approximately 10 OD of
553 logarithmically cells were induced in 5 ml of SD+G (synthetic defined with ammonium as
554 nitrogen source and 2 % galactose as carbon source) for 1 hour. Cells were collected and washed
555 once in ddH_20. Cells were resuspended in 150 µl lysis buffer (0.8 M sorbitol; 10 mM MOPS,
556 pH 7.2; 2 mM EDTA; 1 mM PMSF; 1X cØmplete, mini, EDTA-free protease inhibitor cocktail,
557 Roche). Cells were lysed by bead beating with 0.5 mm glass beads for 3x20s at 6.5 m/s in a
558 benchtop homogenizer (Fastprep-24, MP Biomedical). The cell lysates were centrifuged at
559 500g for 10 min and 25 µl of the resulting supernatant was diluted 1:1 with 2x sample buffer.
560 Proteins were separated using SDS-PAGE and blotted onto Amersham Protran 0.45 µm
561 nitrocellulose membrane (GE Healthcare). The primary antibody and dilution used was rat anti-
562 HA-HRP 3F10 (Roche Applied Science), 1:2500-1:5000. Immunoreactive bands were
563 visualized by chemiluminescence using (SuperSignal West Dura Extended-Duration Substrate;
564 Thermo Fisher Scientific) as substrate in a ChemiDoc imaging system (Biorad).

565

566 **Protease protection assay**

567 Cells were pre-grown in SD+R (synthetic defined with ammonium as nitrogen source and 2 %
568 raffinose and 0.1 % glucose as carbon source) to logarithmic phase. Approximately 5 OD of
569 logarithmically cells were induced in 5 ml of SD+G (synthetic defined with ammonium as
570 nitrogen source and 2 % galactose as carbon source) for 1 hour. Cells were collected and washed
571 once in ddH_20. Cells were resuspended in 150 µl lysis buffer (0.8 M sorbitol; 10 mM MOPS,
572 pH 7.2; 2 mM EDTA; 1 mM PMSF; 1X cØmplete, mini, EDTA-free protease inhibitor cocktail,
573 Roche). Cells were lysed by bead beating with 0.5 mm glass beads for 3x20s at 6.5 m/s in a
574 benchtop homogenizer (Fastprep-24, MP Biomedical). The cell lysates were centrifuged at
575 500g for 10 min and 100 µl of the resulting supernatant was centrifuged at 100 000 g for 30
576 minutes. The membrane pellet was resuspended in 50 µl lysis buffer (0.8 M sorbitol; 10 mM
577 MOPS, pH 7.2; 2 mM EDTA; 5 mM $CaCl_2$). The resulting membrane preparations were
578 digested with 20 µg Proteinase K (Thermo Fisher Scientific) on ice with 0.2 % NP-40 as

indicated. Time points where taken at 0 and 2 h. Proteins were precipitated using trichloroacetic acid as described previously (Silve *et al.*, 1991). Proteins were separated using SDS-PAGE and blotted onto Amersham Protran 0.45 µm nitrocellulose membrane (GE Healthcare). The primary antibodies and dilutions used were, rat anti-HA-HRP 3F10 (Roche Applied Science), 1:2500-1:5000 and rabbit anti-Kar2, 1:5000. Secondary antibody and dilution used was goat anti-rabbit-poly-HRP (Thermo Fisher Scientific), 1:5000. Immunoreactive bands were visualized by chemiluminescence using (SuperSignal West Dura Extended-Duration Substrate; Thermo Fisher Scientific) as substrate in a ChemiDoc imaging system (Biorad).

Acknowledgements

We thank the members of the Ljungdahl laboratory and Claes Andréasson for constructive comments throughout the course of this work. In particular we acknowledge Nina Horwege, and Carlos Sacristán for early contributions in creating plasmid constructs. This research was supported by funding from Swedish Research Council (P.O.L.), Grant/Award numbers: 2011-5925 and 2015-04202.

Competing interests

The authors have no conflicts of interest to report.

References

Andréasson, C., and Ljungdahl, P.O. (2002). Receptor-mediated endoproteolytic activation of two transcription factors in yeast. Genes Dev. *16*, 3158-3172.

Andréasson, C., Neve, E.P.A., and Ljungdahl, P.O. (2004). Four permeases import proline and the toxic proline analogue azetidine-2-carboxylate into yeast. Yeast *21*, 193-199.

Bai, L., You, Q., Feng, X., Kovach, A., and Li, H. (2020). Structure of the ER membrane complex, a transmembrane-domain insertase. Nature *584*, 475-478. 10.1038/s41586-020-2389-3.

Chitwood, P.J., and Hegde, R.S. (2020). An intramembrane chaperone complex facilitates membrane protein biogenesis. Nature *584*, 630-634. 10.1038/s41586-020-2624-y.

Dalbey, R.E., and Kuhn, A. (2014). How YidC inserts and folds proteins across a membrane. Nat Struct Mol Biol *21*, 435-436. 10.1038/nsmb.2823.

Didion, T., Regenberg, B., Jørgensen, M.U., Kielland-Brandt, M.C., and Andersen, H.A. (1998). The permease homologue Ssy1p controls the expression of amino acid and peptide transporter genes in *Saccharomyces cerevisiae*. Mol. Microbiol. *27*, 643-650.

Drozdetskiy, A., Cole, C., Procter, J., and Barton, G.J. (2015). JPred4: a protein secondary structure prediction server. Nucleic Acids Res *43*, W389-394. 10.1093/nar/gkv332.

615 Erpapazoglou, Z., Kafasla, P., and Sophianopoulou, V. (2006). The product of the SHR3
616 orthologue of Aspergillus nidulans has restricted range of amino acid transporter targets.
617 Fungal Genet Biol *43*, 222-233. 10.1016/j.fgb.2005.11.006.

618 Fotiadis, D., Kanai, Y., and Palacin, M. (2013). The SLC3 and SLC7 families of amino acid
619 transporters. Mol Aspects Med *34*, 139-158. 10.1016/j.mam.2012.10.007.

620 Gao, X., Zhou, L., Jiao, X., Lu, F., Yan, C., Zeng, X., Wang, J., and Shi, Y. (2010). Mechanism of
621 substrate recognition and transport by an amino acid antiporter. Nature *463*, 828-832.
622 10.1038/nature08741.

623 Ghaddar, K., Krammer, E.M., Mihajlovic, N., Brohee, S., Andre, B., and Prevost, M. (2014a).
624 Converting the yeast arginine can1 permease to a lysine permease. J Biol Chem *289*, 7232-
625 7246. 10.1074/jbc.M113.525915.

626 Ghaddar, K., Merhi, A., Saliba, E., Krammer, E.M., Prevost, M., and Andre, B. (2014b).
627 Substrate-induced ubiquitylation and endocytosis of yeast amino acid permeases. Mol
628 Cell Biol *34*, 4447-4463. 10.1128/MCB.00699-14.

629 Gilstring, C.F., and Ljungdahl, P.O. (2000). A method for determining the in vivo topology
630 of yeast polytopic membrane proteins demonstrates that Gap1p fully integrates into the
631 membrane independently of Shr3p. J. Biol. Chem. *275*, 31488-31495.

632 Gilstring, C.F., Melin-Larsson, M., and Ljungdahl, P.O. (1999). Shr3p mediates specific
633 COPII coatomer-cargo interactions required for the packaging of amino acid permeases
634 into ER-derived transport vesicles. Mol. Biol. Cell *10*, 3549-3565.

635 Grenson, M., Hou, C., and Crabeel, M. (1970). Multiplicity of the amino acid permeases in
636 Saccharomyces cerevisiae. IV. Evidence for a general amino acid permease. J Bacteriol
637 *103*, 770-777.

638 Gresham, D., Usaite, R., Germann, S.M., Lisby, M., Botstein, D., and Regenberg, B. (2010).
639 Adaptation to diverse nitrogen-limited environments by deletion or extrachromosomal
640 element formation of the GAP1 locus. Proc Natl Acad Sci U S A *107*, 18551-18556.
641 10.1073/pnas.1014023107.

642 Heinrich, S.U., Mothes, W., Brunner, J., and Rapoport, T.A. (2000). The Sec61 complex
643 mediates the integration of a membrane protein by allowing lipid partitioning of the
644 transmembrane domain. Cell *102*, 233-244.

645 Heinrich, S.U., and Rapoport, T.A. (2003). Cooperation of transmembrane segments
646 during the integration of a double-spanning protein into the ER membrane. Embo J *22*,
647 3654-3663.

648 Hou, B., Lin, P.J., and Johnson, A.E. (2012). Membrane protein TM segments are retained
649 at the translocon during integration until the nascent chain cues FRET-detected release
650 into bulk lipid. Mol Cell *48*, 398-408. 10.1016/j.molcel.2012.08.023.

651 Iraqui, I., Vissers, S., Bernard, F., de Craene, J.O., Boles, E., Urrestarazu, A., and André, B.
652 (1999). Amino acid signaling in *Saccharomyces cerevisiae*: a permease-like sensor of
653 external amino acids and F-Box protein Grr1p are required for transcriptional induction

654 of the *AGP1* gene, which encodes a broad-specificity amino acid permease. Mol. Cell. Biol.
655 *19*, 989-1001.

656 Jack, D.L., Paulsen, I.T., and Saier, M.H. (2000). The amino acid/polyamine/organocation
657 (APC) superfamily of transporters specific for amino acids, polyamines and
658 organocations. Microbiology *146 (Pt 8)*, 1797-1814. 10.1099/00221287-146-8-1797.

659 Johnson, A.E., and van Waes, M.A. (1999). The translocon: a dynamic gateway at the ER
660 membrane. Annu Rev Cell Dev Biol *15*, 799-842. 10.1146/annurev.cellbio.15.1.799.

661 Johnsson, N. (2002). A split-ubiquitin-based assay detects the influence of mutations on
662 the conformational stability of the p53 DNA binding domain in vivo. FEBS Lett *531*, 259-
663 264. S0014579302035330 [pii].

664 Johnsson, N., and Varshavsky, A. (1994). Split ubiquitin as a sensor of protein interactions
665 in vivo. Proc Natl Acad Sci U S A *91*, 10340-10344.

666 Jørgensen, M.U., Bruun, M.B., Didion, T., and Kielland-Brandt, M.C. (1998). Mutations in
667 five loci affecting GAP1-independent uptake of neutral amino acids in yeast. Yeast *14*, 103-
668 114.

669 Kanda, N., and Abe, F. (2013). Structural and functional implications of the yeast high-
670 affinity tryptophan permease Tat2. Biochemistry *52*, 4296-4307. 10.1021/bi4004638.

671 Klasson, H., Fink, G.R., and Ljungdahl, P.O. (1999). Ssy1p and Ptr3p are plasma membrane
672 components of a yeast system that senses extracellular amino acids. Mol Cell Biol *19*,
673 5405-5416.

674 Kota, J., Gilstring, C.F., and Ljungdahl, P.O. (2007). Membrane chaperone Shr3 assists in
675 folding amino acid permeases preventing precocious ERAD. J Cell Biol *176*, 617-628.
676 10.1083/jcb.200612100.

677 Kota, J., and Ljungdahl, P.O. (2005). Specialized membrane-localized chaperones prevent
678 aggregation of polytopic proteins in the ER. J Cell Biol *168*, 79-88.

679 Kuehn, M.J., Herrmann, J.M., and Schekman, R. (1998). COPII-cargo interactions direct
680 protein sorting into ER-derived transport vesicles. Nature *391*, 187-190.

681 Kuehn, M.J., Schekman, R., and Ljungdahl, P.O. (1996). Amino acid permeases require
682 COPII components and the ER resident membrane protein Shr3p for packaging into
683 transport vesicles in vitro. J. Cell Biol. *135*, 585-595.

684 Lau, W.T., Howson, R.W., Malkus, P., Schekman, R., and O'Shea, E.K. (2000). Pho86p, an
685 endoplasmic reticulum (ER) resident protein in *Saccharomyces cerevisiae*, is required for
686 ER exit of the high-affinity phosphate transporter Pho84p. Proc. Natl. Acad. Sci. USA *97*,
687 1107-1112.

688 Ljungdahl, P.O., and Daignan-Fornier, B. (2012). Regulation of amino acid, nucleotide, and
689 phosphate metabolism in Saccharomyces cerevisiae. Genetics *190*, 885-929.
690 10.1534/genetics.111.133306.

691 Ljungdahl, P.O., Gimeno, C.J., Styles, C.A., and Fink, G.R. (1992). SHR3: A novel component
692 of the secretory pathway specifically required for the localization of amino acid
693 permeases in yeast. Cell *71*, 463-478.

694 Luo, W.J., Gong, X.H., and Chang, A. (2002). An ER membrane protein, Sop4, facilitates ER
695 export of the yeast plasma membrane [H+]ATPase, Pma1. Traffic *3*, 730-739.
696 10.1034/j.1600-0854.2002.31005.x.

697 Madeira, F., Park, Y.M., Lee, J., Buso, N., Gur, T., Madhusoodanan, N., Basutkar, P., Tivey,
698 A.R.N., Potter, S.C., Finn, R.D., and Lopez, R. (2019). The EMBL-EBI search and sequence
699 analysis tools APIs in 2019. Nucleic Acids Research *47*, W636-W641.
700 https://doi.org/10.1093/nar/gkz268.

701 Malkus, P., Jiang, F., and Schekman, R. (2002). Concentrative sorting of secretory cargo
702 proteins into COPII-coated vesicles. J. Cell Biol. *159*, 915-921.

703 Martínez, P., and Ljungdahl, P.O. (2000). The SHR3 homologue from *S. pombe*
704 demonstrates a conserved function of ER packaging chaperones. J. Cell Sci. *113*, 4351-
705 4362.

706 Martínez, P., and Ljungdahl, P.O. (2004). An ER packaging chaperone determines the
707 amino acid uptake capacity and virulence of *Candida albicans*. Mol Microbiol *51*, 371-384.

708 Miller, E., Antonny, B., Hamamoto, S., and Schekman, R. (2002). Cargo selection into COPII
709 vesicles is driven by the Sec24p subunit. EMBO J. *21*, 6105-6113.

710 Miller, E.A., Beilharz, T.H., Malkus, P.N., Lee, M.C., Hamamoto, S., Orci, L., and Schekman, R.
711 (2003). Multiple cargo binding sites on the COPII subunit Sec24p ensure capture of
712 diverse membrane proteins into transport vesicles. Cell *114*, 497-509.

713 Miller-Vedam, L.E., Brauning, B., Popova, K.D., Schirle Oakdale, N.T., Bonnar, J.L., Prabu,
714 J.R., Boydston, E.A., Sevillano, N., Shurtleff, M.J., Stroud, R.M., et al. (2020). Structural and
715 mechanistic basis of the EMC-dependent biogenesis of distinct transmembrane clients.
716 Elife *9*. 10.7554/eLife.62611.

717 Nagamori, S., Smirnova, I.N., and Kaback, H.R. (2004). Role of YidC in folding of polytopic
718 membrane proteins. J. Cell Biol. *165*, 53-62.

719 O'Donnell, J.P., Phillips, B.P., Yagita, Y., Juszkiewicz, S., Wagner, A., Malinverni, D., Keenan,
720 R.J., Miller, E.A., and Hegde, R.S. (2020). The architecture of EMC reveals a path for
721 membrane protein insertion. Elife *9*. 10.7554/eLife.57887.

722 O'Keefe, S., and High, S. (2020). Membrane translocation at the ER: with a little help from
723 my friends. FEBS J. 10.1111/febs.15309.

724 Ono, B.I., Ishino, Y., and Shinoda, S. (1983). Nonsense mutations in the can1 locus of
725 Saccharomyces cerevisiae. J Bacteriol *154*, 1476-1479.

726 Pleiner, T., Tomaleri, G.P., Januszyk, K., Inglis, A.J., Hazu, M., and Voorhees, R.M. (2020).
727 Structural basis for membrane insertion by the human ER membrane protein complex.
728 Science *369*, 433-436. 10.1126/science.abb5008.

729 Rapoport, T.A., Li, L., and Park, E. (2017). Structural and Mechanistic Insights into Protein
730 Translocation. Annu Rev Cell Dev Biol *33*, 369-390. 10.1146/annurev-cellbio-100616-
731 060439.

732 Risinger, A.L., Cain, N.E., Chen, E.J., and Kaiser, C.A. (2006). Activity-dependent reversible
733 inactivation of the general amino acid permease. Mol Biol Cell *17*, 4411-4419.
734 10.1091/mbc.e06-06-0506.

735 Rosell, A., Meury, M., Alvarez-Marimon, E., Costa, M., Perez-Cano, L., Zorzano, A.,
736 Fernandez-Recio, J., Palacin, M., and Fotiadis, D. (2014). Structural bases for the
737 interaction and stabilization of the human amino acid transporter LAT2 with its ancillary
738 protein 4F2hc. Proc Natl Acad Sci U S A *111*, 2966-2971. 10.1073/pnas.1323779111.

739 Rytka, J. (1975). Positive selection of general amino acid permease mutants in
740 Saccharomyces cerevisiae. J Bacteriol *121*, 562-570.

741 Saier, M.H., Jr. (2000). Families of transmembrane transporters selective for amino acids
742 and their derivatives. Microbiology *146 (Pt 8)*, 1775-1795. 10.1099/00221287-146-8-
743 1775.

744 Schoebel, S., Mi, W., Stein, A., Ovchinnikov, S., Pavlovicz, R., DiMaio, F., Baker, D., Chambers,
745 M.G., Su, H., Li, D., et al. (2017). Cryo-EM structure of the protein-conducting ERAD channel
746 Hrd1 in complex with Hrd3. Nature *548*, 352-355. 10.1038/nature23314.

747 Seinen, A.B., and Driessen, A.J.M. (2019). Single-Molecule Studies on the Protein
748 Translocon. Annu Rev Biophys *48*, 185-207. 10.1146/annurev-biophys-052118-115352.

749 Serdiuk, T., Balasubramaniam, D., Sugihara, J., Mari, S.A., Kaback, H.R., and Muller, D.J.
750 (2016). YidC assists the stepwise and stochastic folding of membrane proteins. Nat Chem
751 Biol *12*, 911-917. 10.1038/nchembio.2169.

752 Serdiuk, T., Steudle, A., Mari, S.A., Manioglu, S., Kaback, H.R., Kuhn, A., and Muller, D.J.
753 (2019). Insertion and folding pathways of single membrane proteins guided by
754 translocases and insertases. Sci Adv *5*, eaau6824. 10.1126/sciadv.aau6824.

755 Sherwood, P.W., and Carlson, M. (1999). Efficient export of the glucose transporter Hxt1p
756 from the endoplasmic reticulum requires Gsf2p. Proc. Natl. Acad. Sci. USA *96*, 7415-7420.

757 Shurtleff, M.J., Itzhak, D.N., Hussmann, J.A., Schirle Oakdale, N.T., Costa, E.A., Jonikas, M.,
758 Weibezahn, J., Popova, K.D., Jan, C.H., Sinitcyn, P., et al. (2018). The ER membrane protein
759 complex interacts cotranslationally to enable biogenesis of multipass membrane proteins.
760 Elife *7*. 10.7554/eLife.37018.

761 Silve, S., Volland, C., Garnier, C., Jund, R., Chevallier, M.R., and Haguenauer-Tsapis, R.
762 (1991). Membrane insertion of uracil permease, a polytopic yeast plasma membrane
763 protein. Mol. Cell. Biol. *11*, 1114-1124.

764 Usami, Y., Uemura, S., Mochizuki, T., Morita, A., Shishido, F., Inokuchi, J., and Abe, F. (2014).
765 Functional mapping and implications of substrate specificity of the yeast high-affinity
766 leucine permease Bap2. Biochim Biophys Acta *1838*, 1719-1729.
767 10.1016/j.bbamem.2014.03.018.

768 van't Klooster, J.S., Bianchi, F., Doorn, R.B., Lorenzon, M., Lusseveld, J.H., Punter, C.M., and
769 Poolman, B. (2020). Extracellular loops matter - subcellular location and function of the
770 lysine transporter Lyp1 from Saccharomyces cerevisiae. FEBS J. 10.1111/febs.15262.

771 Volkmar, N., and Christianson, J.C. (2020). Squaring the EMC - how promoting membrane
772 protein biogenesis impacts cellular functions and organismal homeostasis. J Cell Sci *133*.
773 10.1242/jcs.243519.

774 Wagner, S., Pop, O.I., Haan, G.J., Baars, L., Koningstein, G., Klepsch, M.M., Genevaux, P.,
775 Luirink, J., and de Gier, J.W. (2008). Biogenesis of MalF and the MalFGK(2) maltose
776 transport complex in Escherichia coli requires YidC. J Biol Chem *283*, 17881-17890.
777 10.1074/jbc.M801481200.

778 Waterhouse, A.M., Procter, J.B., Martin, D.M., Clamp, M., and Barton, G.J. (2009). Jalview
779 Version 2--a multiple sequence alignment editor and analysis workbench. Bioinformatics
780 *25*, 1189-1191. 10.1093/bioinformatics/btp033.

781 Wong, F.H., Chen, J.S., Reddy, V., Day, J.L., Shlykov, M.A., Wakabayashi, S.T., and Saier, M.H.,
782 Jr. (2012). The amino acid-polyamine-organocation superfamily. J Mol Microbiol
783 Biotechnol *22*, 105-113. 10.1159/000338542.

784 Zhu, L., Kaback, H.R., and Dalbey, R.E. (2013). YidC protein, a molecular chaperone for
785 LacY protein folding via the SecYEG protein machinery. J Biol Chem *288*, 28180-28194.
786 10.1074/jbc.M113.491613.

787

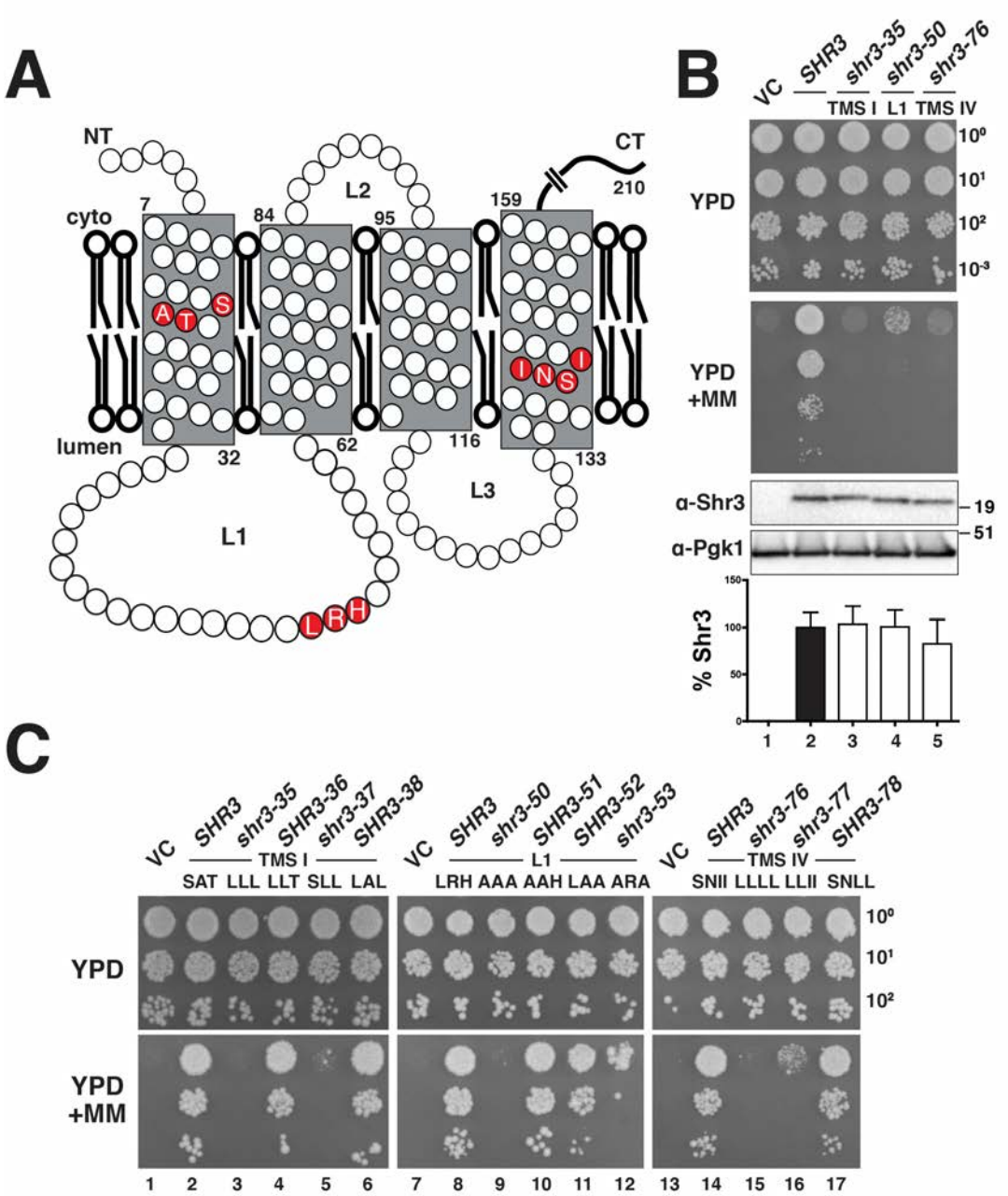

Figure 1. Scanning mutagenesis of the Shr3 membrane domain

(A) Graphical representation of Shr3 topology and position of residues resulting in a non-functional protein. (B) Top: Serial dilutions of cell suspensions from strain JKY2 (*shr3*Δ) carrying pRS316 (VC), pPL210 (*SHR3*), pAR4 (*shr3-35*), pAR18 (*shr3-50*) or pPL1349 (*shr3-76*) spotted on YPD and YPD+MM. The plates were incubated at 30 °C for 2 d and photographed. Bottom: Immunoblot analysis of Shr3 proteins in extracts prepared from the strains; the levels of Pgk1 were used as loading controls. The blots were developed using α-Shr3 and α-Pgk1 antibodies. The signal intensities of the immunoreactive forms of Shr3 and Pgk1 were quantified, and the Shr3 signals were normalized with respect to Pgk1; the mean values are plotted, error bars show standard deviation (n=3). (C) Serial dilutions of cell suspensions from strain JKY2 (*shr3*Δ) carrying pRS316 (VC), pPL210 (*SHR3*), pAR4 (*shr3-35*), pPL1330 (*SHR3-36*), pAR47 (*shr3-37*), pAR37 (*SHR3-38*), pAR18 (*shr3-50*), pAR51 (*SHR3-51*), pAR52 (*SHR3-52*), pAR50 (*shr3-53*), pPL1349 (*shr3-76*), pAR48 (*shr3-77*) or pAR49 (*SHR3-78*) spotted on YPD and YPD+MM plates. Plates were incubated at 30 °C for 2 d and photographed.

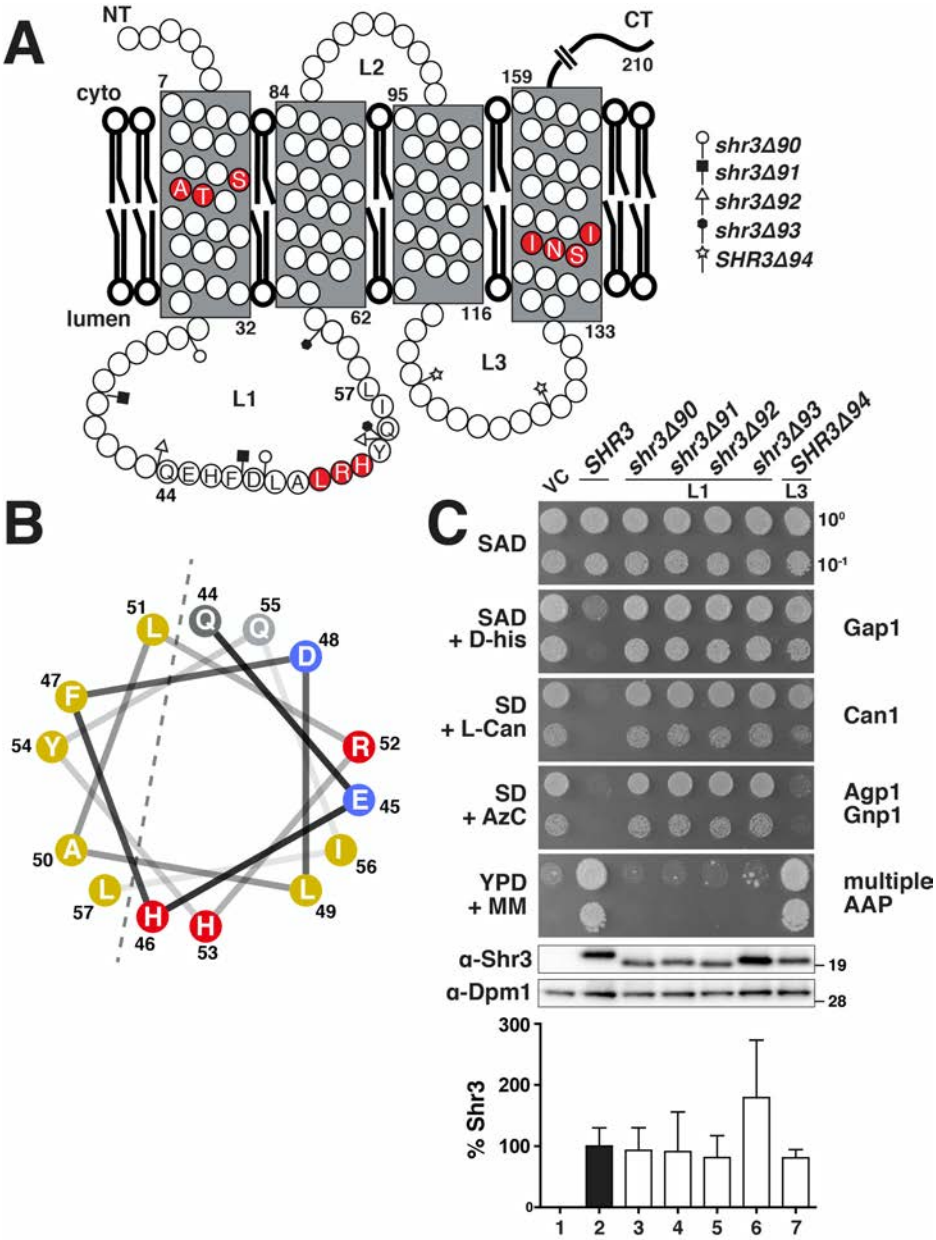

Figure 2. Deletion analysis of ER-lumen oriented loops

(A) Graphical representation of Shr3 topology and the positions of the internal deletions in loops L1 and L3. (B) Based on structural predictions (Drozdetskiy et al., 2015), amino acid residues 44-57 in L1 are predicted to fold into an α-helix with amphipathic character. Helical wheel projection of the L1 α-helix with non-polar (yellow), polar (grey), negatively- (blue) and positively-charged (red) residues indicated. (C) Serial dilutions of cell suspensions from strain JKY2 (*shr3*Δ) carrying pRS316 (VC), pPL210 (*SHR3*), pAR41 (*shr3Δ90*), pAR42 (*shr3Δ91*), pAR43 (*shr3Δ92*), pAR44 (*shr3Δ93*) or pAR45 (*shr3Δ94*) spotted on SAD containing D-histidine (D-his), SD + L-canavanine (L-Can), SD + AzC, and YPD + MM plates. Plates were incubated at 30 °C for 2 d and photographed. Bottom: Immunoblot analysis of Shr3 proteins in extracts prepared from the strains; the levels of Dpm1 were used as loading controls. The blots were developed using α-Shr3 and α-Dpm1 antibodies. The signal intensities of the immunoreactive forms of Shr3 and Dpm1 were quantified, and the Shr3 signals were normalized with respect to Dpm1; the mean values are plotted, error bars show standard deviation (n=3).

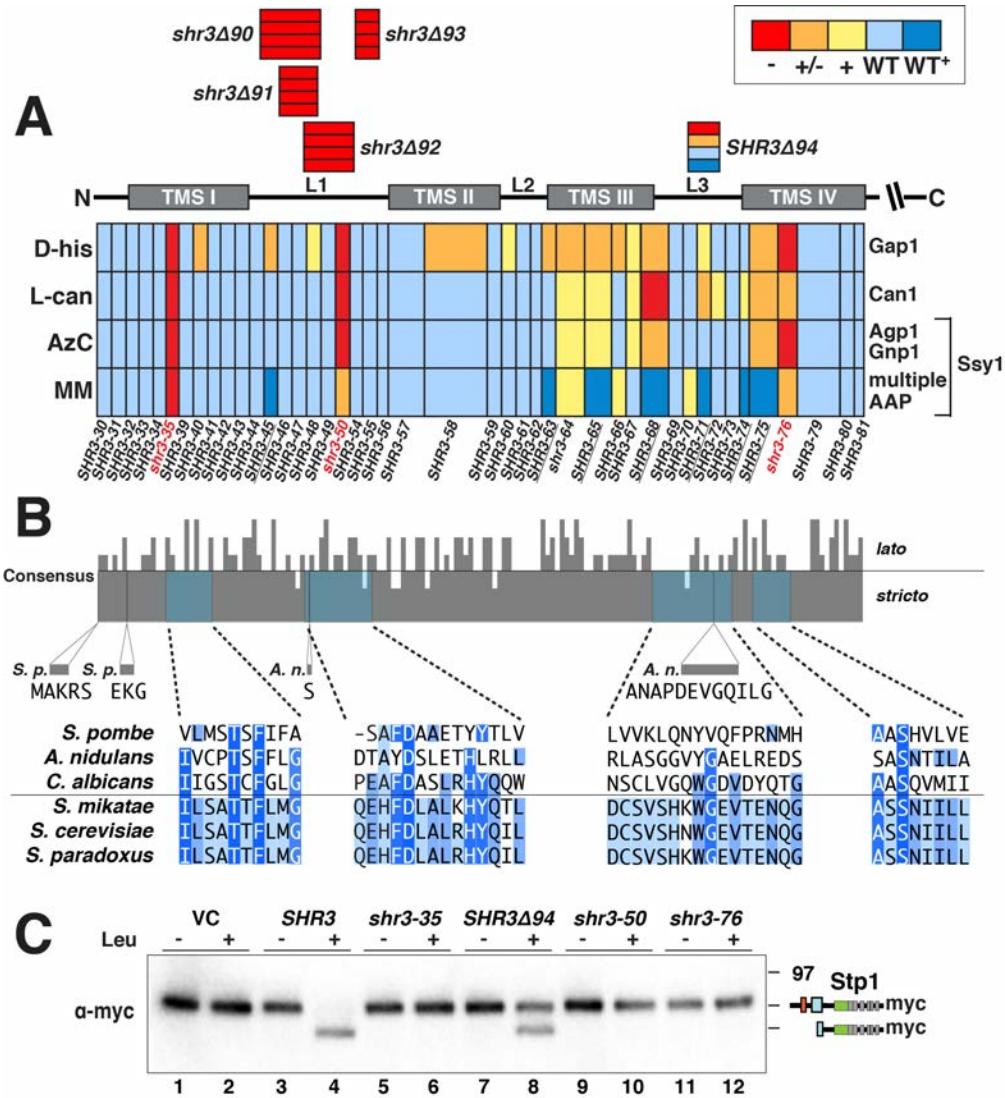

Figure 3. Mutational analysis of Shr3 function and substrate specificity

(A) Summary of growth characteristics of JKY2 (*shr3*Δ) individually expressing 44 Shr3-mutant proteins. Cells were spotted on media containing toxic amino analogues and nitrogen sources as follows: D-his, D-histidine (0.5% w/v), allantoin; L-can, L-canavanine (1 µg/ml), ammonium; AzC, azetidine-2-carboxylate (1 mM), ammonium; MM (200 µg/ml), yeast extract and peptone. Growth was scored after 2 - 3 d of incubation at 30 °C (Supplementary Materials Fig. S1-S10). Colors reflect Shr3 function relative to wildtype activity: red, no function (-); orange, weak but detectable function (+/-); yellow, intermediate function but less than wildtype (+); light blue, wildtype function (WT); dark blue, enhanced function (WT^{+}). (B) Clustal O (Madeira *et al.*, 2019) comparison of Shr3 sequences, corresponding to aa residues 1-159 of *S. cerevisiae*, and orthologs of members from the *Saccharomyces sensu stricto* group (*S. paradoxus*, *S. mikatae*) and orthologs from *sensu lato* fungi (*S. pombe, A. nidulans,* and *C. albicans*). The consensus plot (identity; (Waterhouse et al., 2009) and detailed multiple sequence alignments are presented for the regions with mutations giving rise to major growth defects on selective media; identical residues in three (light blue), four (blue), and five or six homologs (dark blue) are highlighted. (C) Shr3-dependent Ssy1 folding and function assessed by Stp1 processing. Immunoblot analysis of extracts from FGY135 (*shr3*Δ) carrying pCA204 (*STP1-13xMYC*) and pRS316 (VC), pPL210 (*SHR3*), pAR004 (*shr3-35*), pAR45 (*SHR3Δ94*), pAR018 (*shr3-50*) or pPL1351 (*shr3-76*). Cells were grown in SD and induced 30 min with 1.3 mM leucine (+) as indicated.

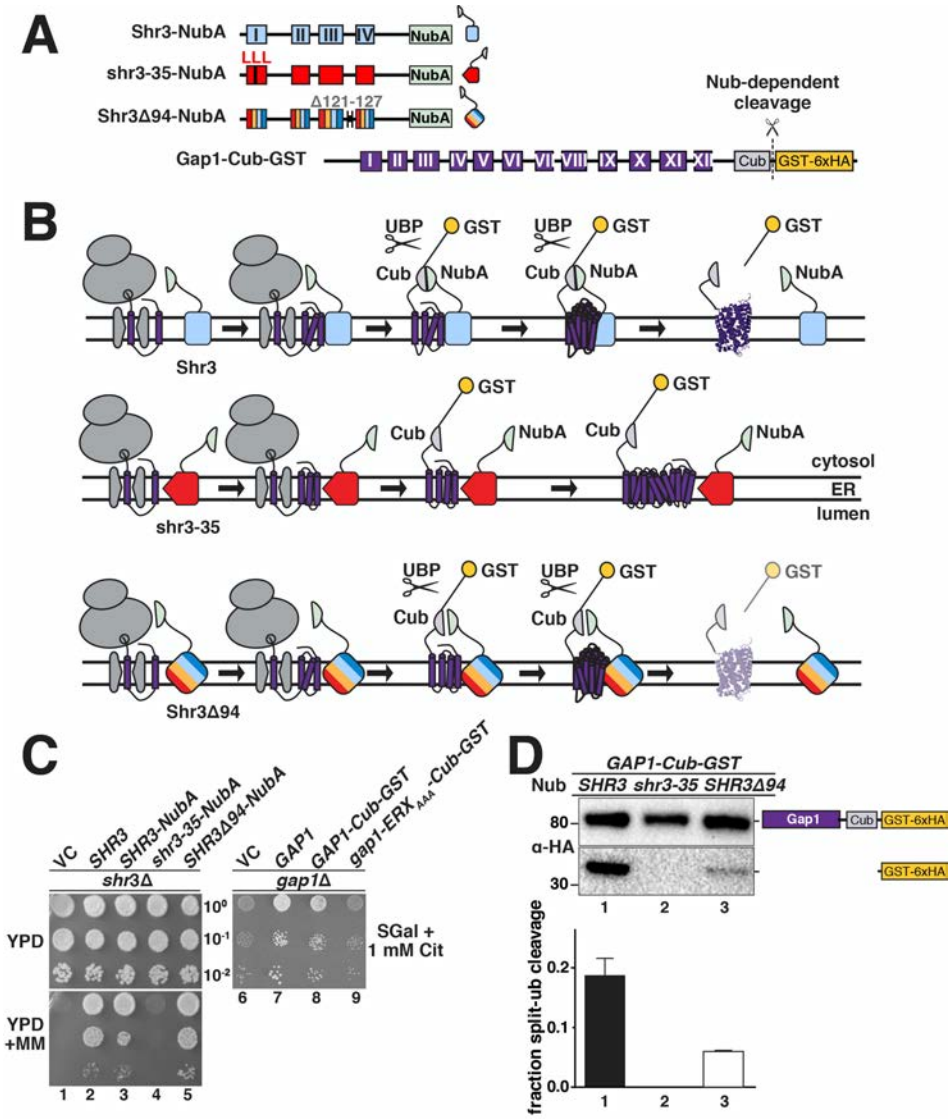

Figure 4. Assessing Shr3-Gap1 interactions using split ubiquitin

(A) Schematic diagram of the split ubiquitin Shr3-NubA, shr3-35-NubA, Shr3Δ94-NubA and Gap1-Cub-GST constructs. (B) Overview of the split-ubiquitin assay and expected outcomes. (C) Left panels: serial dilutions of cell suspensions from strain JKY2 (*shr3*Δ) carrying pRS316 (VC), pPL210 (*SHR3*), pPL1262 (*SHR3-NubA*), pAR67 (*shr3-35-NubA*) or pAR76 (*SHR3Δ94-NubA*) spotted on YPD and YPD+MM plates. Plates were incubated at 30 °C for 2 d and photographed. Right panel: serial dilutions of cell suspensions from strain FGY15 (*gap1*Δ) carrying pRS317 (VC), pJK92 (*GAP1*), pPL1257 (*GAP1-Cub-GST*) or pIM28 (*gap1-ERX*$_{AAA}$*-Cub-GST*) were spotted on minimal medium with 2 % galactose as carbon source and 1 mM L-citrulline as sole nitrogen source. Plates were incubated for 7 d and photographed. (D) Strain FGY135 (*gap1*Δ *shr3*Δ) expressing *SHR3-NubA* (pPL1262), *shr3-35-NubA* (pAR67) or *SHR3Δ94-NubA* (pAR76) and carrying pPL1257 (*GAP1-Cub-GST*) were induced with 2% galactose for 1 h. Proteins extracts were prepared, separated by SDS-PAGE and analyzed by immunoblotting using α-HA antibody. The signal intensities of the immunoreactive forms of full-length and cleaved Gap1 were quantified. The fraction of split-ubiquitin cleavage was determined; the mean values plotted with error bars showing standard deviation (n=3).

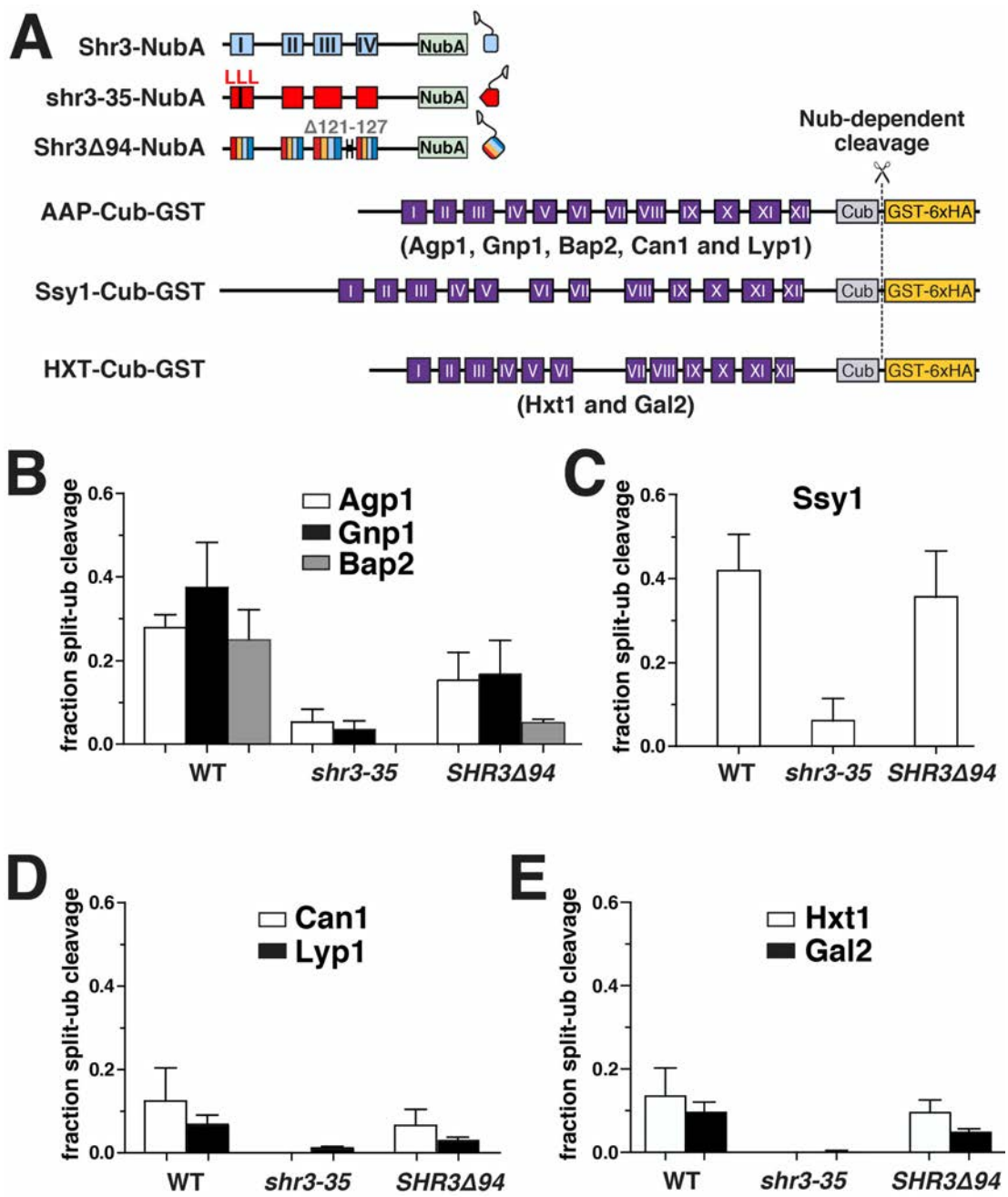

Figure 5. Monitoring Shr3-AAP interactions *in vivo*

(A) Schematic diagram of the split ubiquitin constructs used to evaluate Shr3-AAP and Shr3-HXT interactions. (B) Shr3-Agp1, Shr3-Gnp1 and Shr3-Bap2 interactions. (C) Shr3-Ssy1 interactions. (D) Shr3-Can1 and Shr3-Lyp1 interactions. (E) Shr3-Hxt1 and Shr3-Gal2 interactions. Strain FGY135 (*gap1*Δ *shr3*Δ) expressing *SHR3-NubA* (pPL1262), *shr3-35-NubA* (pAR67) or *SHR3Δ94-NubA* (pAR76) and carrying (B) pIM6 (*AGP1-Cub-GST*), pIM17 (*GNP1-Cub-GST*), or pIM7 (*BAP2-Cub-GST*) or (C) pIM19 (*SSY1-Cub-GST*) or (D) pIM8 (*CAN1-Cub-GST*) or pIM18 (*LYP1-Cub-GST*), or (E) pIM32 (*HXT1-Cub-GST*) or pIM33 (*GAL2-Cub-GST*) were induced with 2% galactose for 1 h. Proteins extracts were prepared, separated by SDS-PAGE and analyzed by immunoblotting using α-HA antibody. The signal intensities of the immunoreactive forms of full-length and cleaved Agp1, Gnp1, Bap2, Ssy1, Can1, Lyp1, Hxt1 and Gal2 constructs were quantified. The fraction of split-ubiquitin cleavage was determined; the mean values plotted with error bars showing standard deviation (n=3).

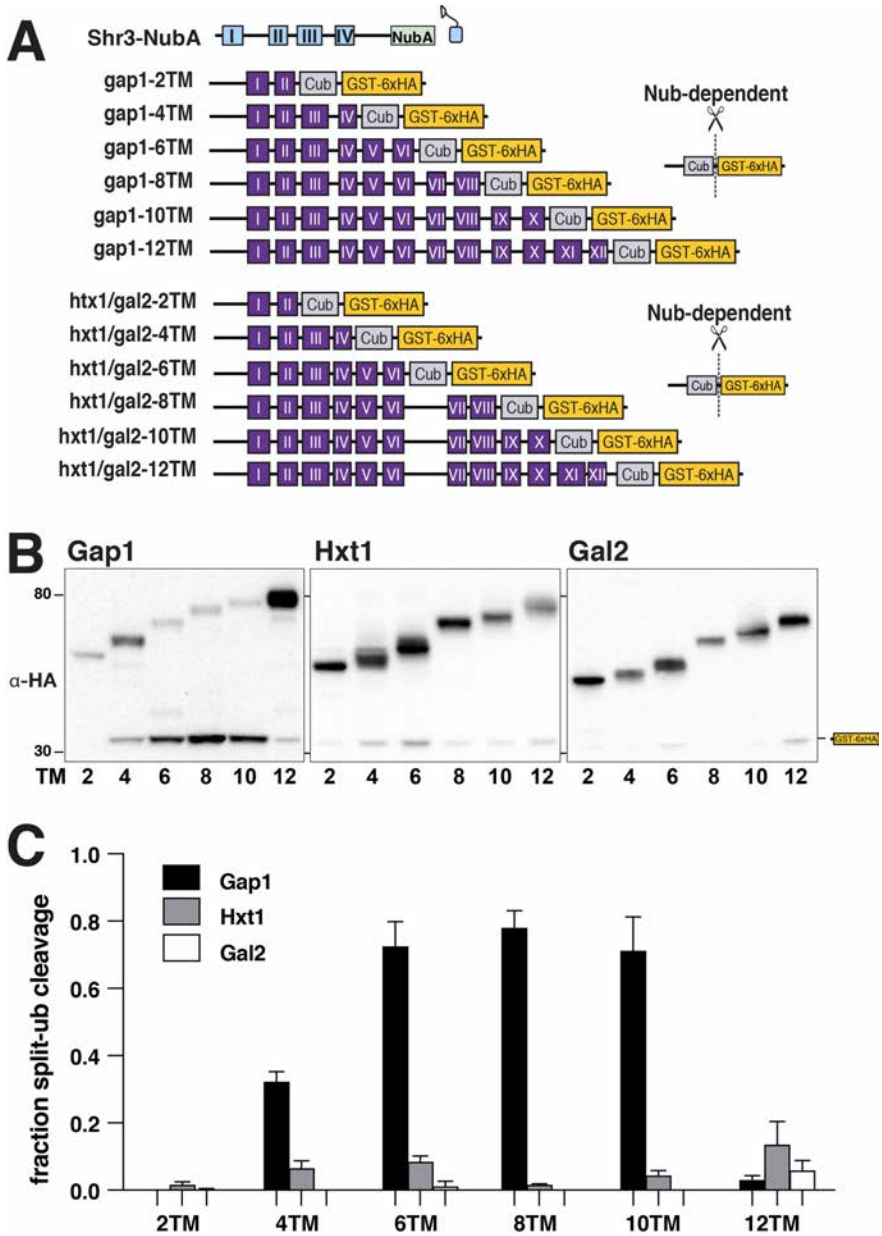

Figure 6. Progressivity of Shr3-Gap1 chaperone-substrate interactions

(A) Schematic diagram of split ubiquitin constructs including the gap1-Cub-GST, hxt1-Cub-GST and gal2-Cub-GST truncation constructs. (B) Strain FGY135 (*gap1*Δ *shr3*Δ) carrying pPL1262 (*SHR3-NubA*) and pIM1 (*gap1-2TM-Cub-GST*), pIM2 (*gap1-4TM-Cub-GST*), pIM3 (*gap1-6TM-Cub-GST*), pIM4 (*gap1-8TM-Cub-GST*), pIM5 (*gap1-10TM-Cub-GST*) or pIM16 (*gap1-12TM-Cub-GST*) (left panel), or pIM34 (*hxt1-2TM-Cub-GST*), pIM35 (*hxt1-4TM-Cub-GST*), pIM36 (*hxt1-6TM-Cub-GST*), pIM37 (*hxt1-8TM-Cub-GST*), pIM38 (*hxt1-10TM-Cub-GST*) or pIM39 (*hxt1-12TM-Cub-GST*) (center panel) or pIM40 (*gal2-2TM-Cub-GST*), pIM41 (*gal2-4TM-Cub-GST*), pIM42 (*gal2-6TM-Cub-GST*), pIM43 (*gal2-8TM-Cub-GST*), pIM44 (*gal2-10TM-Cub-GST*) or pIM45 (*gal2-12TM-Cub-GST*) (right panel) were induced with 2% galactose for 1 h. Extracts were prepared, separated by SDS-PAGE and analyzed by immunoblotting using α-HA antibody. (C) The signal intensities of the immunoreactive forms of uncleaved Cub constructs and cleaved interaction marker (GST-6xHA) were quantified; the mean values of the fraction of split ubiquitin cleavage is plotted with error bars showing standard deviation (n=3).

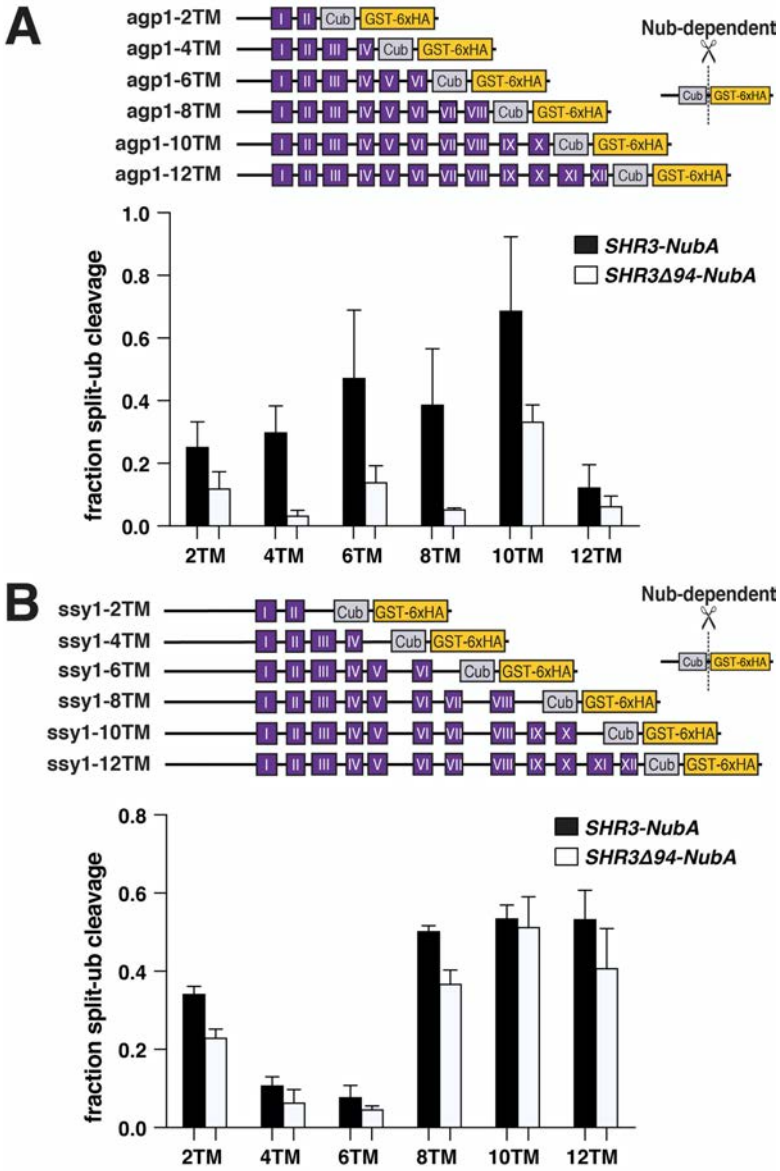

Figure 7. Progressive Shr3-Agp1 and Shr3-Ssy1 chaperone-substrate interactions

(A) Schematic diagram of agp1-Cub-GST truncation constructs. Strain FGY135 (*gap1*Δ *shr3*Δ) expressing *SHR3-NubA* (pPL1262) or *SHR3*Δ*94-NubA* (pAR76) and carrying pIM9 (*agp1-2TM-Cub-GST*), pIM10 (*agp1-4TM-Cub-GST*), pIM11 (*agp1-6TM-Cub-GST*), pIM12 (*agp1-8TM-Cub-GST*), pIM13 (*agp1-10TM-Cub-GST*) or pIM26 (*agp1-12TM-Cub-GST*) were induced with 2% galactose for 1 h. Extracts were prepared, separated by SDS-PAGE and analyzed by immunoblotting using α-HA antibody. The signal intensities of the immunoreactive forms of uncleaved Cub constructs and cleaved interaction marker (GST-6xHA) were quantified; the mean values of the fraction of split ubiquitin cleavage is plotted with error bars showing standard deviation (n=3). (B) Schematic diagram of ssy1-Cub-GST truncation constructs. Strain FGY135 (*gap1*Δ *shr3*Δ) expressing *SHR3-NubA* (pPL1262) or *SHR3*Δ*94-NubA* (pAR76) and carrying pIM20 (*ssy1-2TM-Cub-GST*), pIM21 (*ssy1-4TM-Cub-GST*), pIM22 (*ssy1-6TM-Cub-GST*), pIM23 (*ssy1-8TM-Cub-GST*), pIM24 (*ssy1-10TM-Cub-GST*) or pIM25 (*ssy1-12TM-Cub-GST*) were induced with 2% galactose for 1 h. Extracts were prepared, and analyzed as in (A) and the mean values of the fraction of split ubiquitin cleavage is plotted with error bars showing standard deviation (n=3).

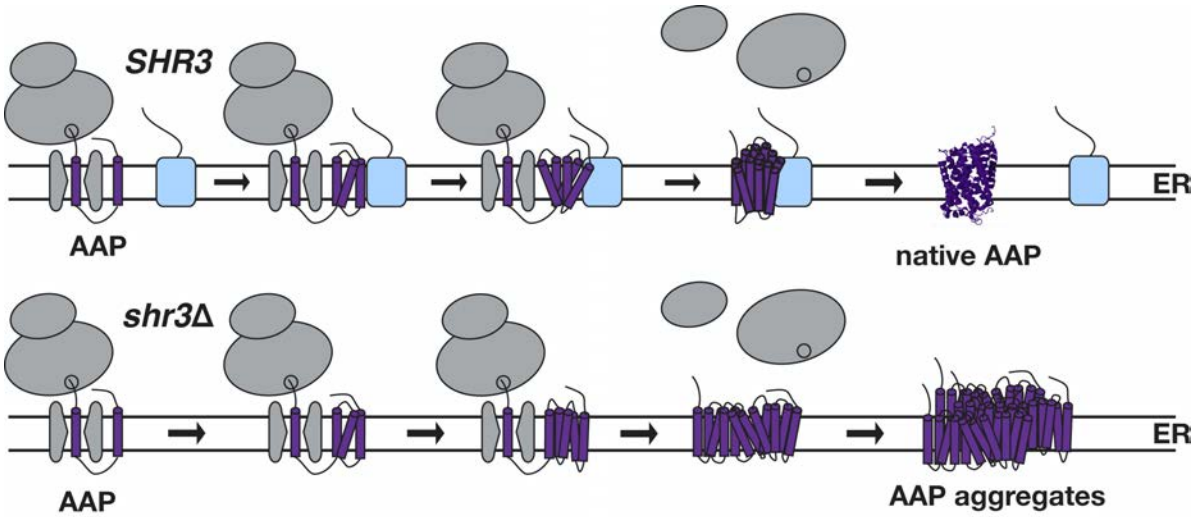

Figure 8. Model of Shr3 facilitated AAP folding

Shr3 interacts transiently with AAP as they are co-translationally inserted into the ER membrane. Interactions start early, when 2-4MS have partitioned into the lipid bilayer, and continue until all MS are inserted. When AAP have fully integrated into the membrane and attain native conformations, the interactions with Shr3 diminish. The co-translational Shr3 function is specifically required for AAP folding and ER-exit. The chaperone activity depends on relatively few residues of the Shr3 sequence, suggesting that it functions as folding template. In the absence of Shr3, AAP are specifically retained in the ER and form high-molecular weight aggregates that are recognized as ERAD substrates.

Supplementary Material

Figures:

Fig S1. Growth-based assessment of Shr3 substrate specificity - I

Fig S2. Growth-based assessment of Shr3 substrate specificity - II

Fig S3. Growth-based assessment of Shr3 substrate specificity - III

Fig S4. Growth-based assessment of Shr3 substrate specificity - IV

Fig S5. Growth-based assessment of Shr3 substrate specificity - V

Fig S6. Growth-based assessment of Shr3 substrate specificity - VI

Fig S7. Growth-based assessment of Shr3 substrate specificity - VII

Fig S8. Growth-based assessment of Shr3 substrate specificity - VIII

Fig S9. Growth-based assessment of Shr3 substrate specificity - IX

Fig S10. Growth-based assessment of Shr3 substrate specificity - X

Fig S11. Effect of ER exit motif mutations on Shr3-AAP interactions

Fig S12. Protease cleavage assay to assess the topology of shr3-35-NubA and gap1-2TM-Cub-GST constructs

Fig S13. Interactions between Shr3-NubA and can1-8TM, -10TM-Cub-GST

Tables:

Table S1. Strains

Table S2. Plasmids